A regulatory circuit involving the NADH dehydrogenase-like complex balances C_4 photosynthetic carbon flow and cellular redox in maize

Qiqi Zhang[1,2], Shilong Tian[2], Genyun Chen[1], Qiming Tang[1,2], Yijing Zhang[3], Andrew J. Fleming[4], Xin-Guang Zhu[1], Peng Wang[1]*

[1] Laboratory of Photosynthesis and Environmental Biology, CAS Center for Excellence in Molecular Plant Sciences (CEMPS), Chinese Academy of Sciences. Shanghai 200032, China
[2] University of Chinese Academy of Sciences, Shanghai 200032, China
[3] State Key Laboratory of Genetic Engineering, Collaborative Innovation Center of Genetics and Development, Department of Biochemistry, Institute of Plant Biology, School of Life Sciences, Fudan University, Shanghai 200438, China
[4] School of Biosciences, University of Sheffield, Western Bank, Sheffield, S10 2TN, UK

* Author for correspondence: Peng Wang
Email: wangpeng@cemps.ac.cn

Summary

- C_4 plants typically operate a CO_2 concentration mechanism from mesophyll (M) cells into bundle sheath (BS) cells. NADH dehydrogenase-like (NDH) complex is enriched in the BS cells of many NADP-ME type C_4 plants, and is more abundant in C_4 than in C_3 plants, but to what extent it is involved in the CO_2 concentration mechanism remains to be experimentally investigated.
- We created maize and rice mutants deficient in NDH function, and used a combination of transcriptomic, proteomic, and metabolomic approaches for comparative analysis.
- Considerable decrease in growth, photosynthetic activities, and levels of key photosynthetic proteins were observed in maize but not rice mutants. However, gene expression for many cyclic electron transport and Calvin-Benson cycle components plus BS specific C_4 enzymes, was up-regulated in maize mutants. Metabolite analysis of the maize *ndh* mutants revealed increased NADPH/NADP ratio, as well as malate, RuBP, FBP, and photorespiration components.
- We suggest that by optimizing NADPH and malate levels, adjusting NADP-ME activity, NDH functions to balance metabolic and redox states in the BS cells of maize, coordinating photosynthetic gene expression and protein content, thus directly regulating the carbon flow in the two-celled C_4 system of maize.

Keywords

Bundle sheath cell, C_4 photosynthesis, CO_2 concentration mechanism, cyclic electron transport, maize, NDH complex, photosynthetic metabolite, redox regulation.

Introduction

Plants use light energy to eventually drive CO_2 assimilation into carbohydrates through photosynthesis. The organization and operation of the photosynthetic apparatus are finely regulated at different levels, and a deeper understanding of them would benefit crop improvement. Rice and wheat are the most widely consumed food crops, but the C_3 photosynthesis in these plants does not operate in an efficient way, with the assimilation of CO_2 considerably compromised due to photorespiration (Bauwe *et al.*, 2010; Raines, 2011). Crops such as maize and sorghum have evolved a distinct and more efficient process, C_4 photosynthesis. Typical C_4 leaves display a special Kranz anatomy: vascular bundles of C_4 maize leaves are sequentially surrounded by functionally differentiated bundle sheath (BS) cells and mesophyll (M) cells, which contain chloroplasts with different ultrastructure and a specific distribution of metabolic enzymes. In C_4 plants, CO_2 is concentrated through intercellular transport of C_4 acids (such as malate and aspartate) from M cells where CO_2 is captured via PEP carboxylase, to the BS cells where Rubisco is present. The C_4 acids are decarboxylated in the BS cells, raising CO_2 concentration around Rubisco, decreasing photorespiration, and thus achieving more efficient assimilation of CO_2 and improved photosynthesis (Furbank, 2017; von Caemmerer *et al.*, 2017).

One distinctive feature of C_4 BS chloroplasts maybe linked to a strong ability to perform cyclic electron transport (CET). CET pathways are mainly mediated by the chloroplast NADH dehydrogenase-like complex (NDH), and by the proton gradient regulatory proteins PGR5 and PGRL1 (Johnson, 2011; Shikanai, 2014; Suorsa, 2015; Yamori *et al.*, 2016). The NDH complex binds to PSI and is specifically distributed in the non-stacking regions of thylakoids (Peng *et al.*, 2008, 2009, 2011; Kouřil *et al.*, 2014; Yadav *et al.*, 2017). By mediating CET from the receptor side of photosystem I (PSI) to plastoquinone (PQ), an NDH-dependent proton gradient is established across the thylakoid membrane to drive ATP synthesis (Wang *et al.*, 2006; Ishikawa *et al.*, 2016b;

Strand *et al.*, 2017). In C_3 plants, CET is not prominent under normal conditions, and CO_2 assimilation is mainly driven by linear photosynthetic electron transport (LET). However, under environmental stresses, such as high temperature, high light and drought, LET is suppressed, while CET via NDH is often up-regulated. This helps to decrease oxidative damage and to replenish ATP (Burrows *et al.*, 1998; Endo *et al.*, 1999; Horváth *et al.*, 2000; Li *et al.*, 2004; Wang *et al.*, 2006; Ishikawa *et al.*, 2008a; Yamori *et al.*, 2011; Suorsa *et al.*, 2015). In the C_4 plant maize, BS chloroplasts lack the stacking grana thylakoids rich in photosystem II (PSII), and instead possess a large number of non-stacking stromal thylakoids rich in PSI and NDH complex (Majeran and van Wijk, 2009; Ermakova *et al.*, 2020). The C_4 plant and cell-specific up-regulation of NDH was confirmed at both transcript and protein levels (Kubicki *et al.*, 1996; Darie *et al.*, 2005, 2006; Takabayashi *et al.*, 2005; Majeran *et al.*, 2008; Friso *et al.*, 2010; Li *et al.*, 2010; Bräutigam *et al.*, 2011). The functional significance of the enriched NDH content in C_4 BS cells has aroused great interest.

It has been noted that NDH content is higher in a variety of C_4 leaves (both NADP-ME and NAD-ME types) than in C_3 leaves, leading to the idea that it offers increased ATP generation required by the C_4 pathway (Ishikawa *et al.*, 2016b). As evidence, studies on several C_4 plants have shown that the NDHH subunit is increased in cell types requiring additional ATP for CO_2 concentration (e.g., BS cells of NADP-ME type and M cells of NAD-ME type leaves) (Takabayashi *et al.*, 2005). In some C_4 species only NDH-mediated CET is enhanced, while in others both NDH and PGR5-PGRL1 pathways are enhanced (Munekage *et al.*, 2010; Nakamura *et al.*, 2013). As highlighted by the involvement of NDH but not PGR5 in the CO_2 concentration mechanism (CCM) of cyanobacteria (Price *et al.*, 2013; Long *et al.*, 2016), whether NDH plays a more specific role apart from ATP production in the C_4 pathway is still unknown. Further clue may be related with the involvement of NDH-CET in

NADPH turnover and redox adjustment. Since various photosynthetic enzymes that take part in light reactions and carbon reactions are regulated via redox components, understanding the different redox needs in the M and BS chloroplasts of C_4 plants is crucial for engineering efficient C_4 photosynthesis (Turkan et al., 2018). Particularly, NADP-malic enzyme (NADP-ME) catalyzes the oxidative decarboxylation of malate to yield CO_2 and pyruvate with the concomitant production of NADPH (Drincovich et al. 2001), being the main source of reducing power for BS chloroplasts in maize. For C_4 photosynthesis to efficiently concentrate CO_2 in BS chloroplasts, the NADP-ME decarboxylation and Rubisco carboxylation rates must be coordinated. Besides having acquired an enriched BS expression, the C_4-type NADP-ME displays a particular redox modulation in maize (Alvarez et al., 2012). Whether or how NDH-CET, as well as the ferredoxin/thioredoxin system, are related to this modulation greatly attract our interest.

Several groups have taken a molecular genetic approach to understand the relationship between NDH-mediated CET and C_4 photosynthesis. Studies have found that mutations in the NDHN or NDHO subunits of maize lead to increased photorespiration and reduced carbon assimilation under high-light and saturated CO_2 conditions (Peterson *et al.*, 2016). In the C_4 species *Flaveria bidentis*, knockout of the NDHN or NDHO subunit, but not PGR5 nor PGRL1, resulted in slow plant growth and decreased CO_2 assimilation (Ishikawa *et al.*, 2016a; Ogawa *et al.*, 2023). These studies indicate that the function of NDH is crucial for photosynthesis and growth of C_4 plants, but the mechanism underlying the phenotype remains to be further studied. In this study, we took a reverse genetic approach and created mutants of selected NDH subunits (NDF6 and NDHU subunits), both in a C_4 crop (maize) and a C_3 crop (rice), then used a combination of transcriptomic, proteomic, and metabolomic approaches to identify the mechanism by which loss of NDH activity in C_4 leaves leads to decreased CO_2 assimilation and growth. Our data

highlight the importance of BS-localized NDH activity in maize for the balancing of carbon flux and redox state between the BS and MS cells, in addition to the generally accepted role of providing ATP. The necessity of this regulation is most prominent in the BS cells, which undergo continuous import of malate and generation of NADPH as an essential part of the C_4 mechanism.

Materials and Methods

Plant growth conditions and trait measurement

Maize plants were grown in 6 L pots with a mix of 60% peat soil and 20% vermiculite. Rice plants were grown in 6 L pots with field soil. The plants were grown in environmentally controlled phytotron room [27 °C in day and 25 °C at night, 600 µmol photons m^{-2} s^{-1} photosynthetic photon flux density (PPFD), 16 h light and 8 h dark photoperiod, and ~70% relative humidity] with normal fertilizer application.

To estimate leaf total chlorophyll content, a SPAD 502 Plus Chlorophyll Meter (Spectrum Technologies) was used. Plant height was measured from the soil surface to the collar of the youngest fully expanded leaf.

Monitoring chlorophyll fluorescence and P700 redox

Post-illumination increase of chlorophyll fluorescence were monitored after turning off the actinic light (200 µmol photons m^{-2} s^{-1}, white light, for 180 sec), using a PAM chlorophyll fluorometer (PAM101, Walz, Germany) attached with emitter-detector assembly and 101ED unit, as previously described (Wang *et al.*, 2006). Fv/Fm, ETR, and NPQ were measured using a PAM-2000 chlorophyll fluorometer (Walz, Germany) according to standard procedures.

The redox kinetics of P700 was recorded using a Dual-PAM-100 instrument (Walz, Germany). Before measurements, the leaves were dark-acclimated for 20 min. Far-red light (30 sec) was applied to start the measurement, and the initial rate of $P700^+$ reduction following termination of

182 far-red light was calculated.

183

184 **Photosynthetic gas exchange measurements**

185 The photosynthetic rate of phytotron-grown plants 60 days after transplanting
186 was measured using LI-6800 (for maize) or LI-6400 (for rice) portable gas
187 exchange systems (LI-COR Biosciences). The temperature, relative humidity,
188 and photosynthetic photon flux density (PPFD) were set at 28 °C, 70%, and
189 1200 μmol $m^{-2}s^{-1}$ respectively for the leaf chamber. CO_2 concentrations were
190 set as 400, 200, 50, 100, 150, 200, 300, 400, 500, 600, 800, 1000, 1200 ppm
191 in a step-wise manner. The A/Ci curve of maize was fitted according to Zhou *et*
192 *al.*, 2019.

193

194 **Blue native (BN)-PAGE and Western blot**

195 Maize leaves were homogenized in cold STN medium (0.4 M sucrose, 50 mM
196 Tris–HCl pH 7.6, 10 mM NaCl). The homogenate was filtered through two
197 layers of nylon cloth and centrifuged at 200 g for 3 min at 4 °C. Supernatant
198 was centrifuged at 5000 g for 10 min at 4°C to pellet crude chloroplasts.
199 Chloroplasts were ruptured in cold TN medium (50 mM Tris–HCl pH 7.6, 10
200 mM NaCl), and thylakoid membranes were separated by centrifugation at
201 8000 g for 5 min at 4°C. The thylakoid membranes were suspended in
202 solubilization buffer [25 mM BisTris-HCl, pH 7.0, 10 mM $MgCl_2$, 20% (v/v)
203 glycerol] at a final chlorophyll concentration of 1 mg ml^{-1}. The thylakoid
204 membranes containing the 0.5 mg ml^{-1} chlorophyll were solubilized with 1.2%
205 (w/v) n-dodecyl-β-maltoside (DDM) by gentle agitation on ice for 1 h. After
206 centrifugation at 15000 g for 10 min at 4°C, the samples were immediately
207 subjected to Native-PAGE and loaded on chlorophyll basis of 5 μg per lane.
208 Electrophoresis was performed at 4 °C by increasing the voltage gradually
209 from 50 up to 200 V during the 5.5 h run. For two-dimensional analysis,
210 excised BN-PAGE lanes were soaked in SDS sample buffer for 10 min,

211 layered onto 12.5% SDS polyacrylamide gels, and electrophoresis was
212 performed at 120 V.

213 For the immunoblot analysis of total proteins, leaves of 4-week-old plants
214 were extracted in SDS sample buffer, and 25 μg of proteins were subjected to
215 SDS-PAGE. The separated total proteins or proteins from two-dimensional
216 gels were subsequently transferred onto polyvinylidene difluoride (PVDF)
217 membranes (Merck, Cat. IPVH00010), hybridized with specific antibodies, and
218 visualized by ECL assay kit (Thermo Scientific) according to the
219 manufacturer's protocol.

220

221 **Paraffin section and I_2-KI staining**

222 Leaf samples were harvested at 7AM and 7PM from 3-week-old plants. The
223 middle portion of the fully expanded leaf was dissected and fixed in
224 formaldehyde-acetic acid-alcohol (FAA) solution under vacuum (20 psi) at
225 room temperature for at least 30min. Leaf sections were dehydrated using an
226 ethanol series from 70% ethanol to 100% ethanol and incubated for 2 hours at
227 each concentration solution. Samples were then infiltrated in varying
228 concentrations of ethanol: histoclear solution (25% histoclear to 100%
229 histoclear) and incubated for 2 hours at each concentration. Subsequently,
230 samples were infiltrated in varying concentrations of histoclear: paraffin
231 solution (25% paraffin to 100% paraffin) for 2 hours at each concentration. The
232 processed samples were placed in heated 100 % paraffin and polymerized for
233 30 min at 4 °C. Embedded samples were cut into 10 μ m thick sections with a
234 microtome (Leica RM2125RTS) and the paraffin sections were mounted on
235 slides. Starch was visualized in leaf sections by iodine potassium iodide (I_2-KI)
236 staining.

237

238 **Histological staining of ROS accumulation**

239 Leaf fragments of 2 cm size from the middle part of fully expanded leaves were

transferred into DAB staining solution (1 mg ml^{-1} DAB, 10 mM Na_2HPO_4, and 0.05% Tween-20), vacuum infiltrated, and incubated for 6 h in the light (200 µmol photons m^{-2} s^{-1}). Chlorophyll was removed by replacing DAB solution with decoloration solution (ethanol : acetic acid : glycerol = 3 : 1 : 1) and incubated at 85 °C. The samples were then processed with paraffin sectioning as described above, and cross sections were examined with light microscopy.

Transmission electron microscopy

Leaf sections of 2 mm size were cut from the middle part of recent fully expanded leaves and fixed in 2.5% glutaraldehyde. The samples were placed in a microcentrifuge tube and low vacuum condition was applied for 60 min at room temperature. Post fixation in osmium tetroxide, embedding in Spurr's resin, and other steps were performed by the technology platform in Center for Excellence in Molecular Plant Sciences, following standard procedures. The ultra-thin sections were imaged at 80 KV with a Hitachi H-7650 transmission electron microscope.

RNA-sequencing

For maize, leaves at the youngest fully expanded stage were sampled, from 30-d-old plants. And for rice, samples were harvested from 60-d-old plants. Each biological replicate consisted of leaves from 4 individual plants, and 3 biological replicates (from 12 plants in total) were sequenced for each sample. Library preparation followed standard procedure, and the libraries were sequenced on Illumina Novaseq 6000 platform using 150-bp paired-end sequencing strategy. The cleaned reads of maize samples were mapped onto the Zm-B73-REFERENCE-NAM-5.0 reference genome, and cleaned reads of rice samples were mapped onto the RAP Gene ID reference genome, both using HISAT2. The differentially expressed genes (DEGs) were identified by DEseq2 (v1.16.1) with definition of fold change more than 2 and false

discovery rate (FDR) <0.01.

Gene expression analysis

Leaf samples were frozen with liquid nitrogen and ground in a tissue grinding machine. RNA was extracted using RNAiso Plus reagent (Takara, Cat. 9108) according to the manufacturer's instructions. To synthesize cDNA, 2 μg RNA was used, with a first strand cDNA synthesis kit (YEASEN, 11141ES60). qRT–PCR was carried out with Hieff UNICON® Universal Blue qPCR SYBR Master Mix (YEASEN, 11184ES08) in a final reaction volume of 20 μL. Relative expression was calculated by comparison to *ZmEF1α* (Hughes and Langdale, 2020) or *OsACTIN*, and data processed using Excel software.

Separation of BS strands

BS strands were isolated using a method modified from Chang *et al*., 2012. Maize leaves were harvested at the same stage for RNA-seq and 5 g of each sample were used to isolate BS strands. Each biological replicate consisted of leaves from 6 individual plants, and 3 biological replicates were used for each sample. Several leaf blades were stacked and cut perpendicularly to the long axis into 0.5- to 1-mm slices with sterilized razor blades and quickly transferred into 50 mL of cold BS cell isolation medium [0.6 M sorbitol, 50 mM Tris-HCl (pH 8.0), 5 mM EDTA, 0.5% polyvinylpyrrolidone-10, 10 mM DTT, and 100 mM 2-mercaptoethanol]. After blending for 10 s twice in a blender at high speed, the mixture was first filtered through a 178 μm mesh and then filter through a 125 μm mesh. The filtration processes were repeated. BS strands that passed through the 125 μm mesh were filtered and retained on a 70 μm mesh, then placed on a paper towel stack to remove excess moisture, and frozen in liquid nitrogen. The purity of BS strands was assessed with a light microscope and M and BS markers (PPDK and Rubisco, respectively) were monitored by Western blot **(Fig. S7c)**.

Mass spectrometry analysis of protein samples

Equal amount of proteins (20 µg) were used for following analysis. Briefly, protein was reduced by 10 mM of TCEP and alkylated by 25 mM of CAA at 37°C in the dark for 1 h. Six volumes of cold acetone were subsequently added. Samples were left to precipitate overnight at -20°C and centrifuged at 12000 rpm for 20 min at 4°C, and supernatants were removed. Resulting pellets were washed twice with 90% cold acetone and suspended in 20 µL of 50 mM NH_4HCO_3. Sequence grade modified trypsin (Promega, Madison, WI) was added at the ratio of 1:20 to digest the proteins at 37°C overnight. The peptide mixture was desalted by C18 ZipTip and dried in a vacuum concentrator at 4°C. For MS analysis, the peptides were dissolved in 0.1% formic acid. Peptides were resolved on an EASY-Spray PepMap RSLC C18 column (Thermo Scientific, 25 cm x 150 µm ID, 2 µm, 55°C) with the following gradient profile delivered at 300 nl min^{-1} by a Dionex RSLCnano chromatography system (Thermo Scientific): 97% solvent A (0.1% formic acid in water) to 8% solvent B (0.1% formic acid in 80% acetonitrile) over 2 min, 8% to 23% solvent B over 90 min, 23% to 40% solvent B over 15 min, then 40% to 100% solvent B over 7min and maintained 8 min. The mass spectrometer was a Q Exactive HF-X hybrid quadrupole-Orbitrap system (ThermoFisher Scientific, MA, USA). Raw Data of DIA were processed and analyzed by Spectronaut 16 (Biognosys AG, Switzerland) with default settings. Maize proteome UP000007305_4577 (UniProt) database was referenced. Proteins entered into subsequent analysis must fulfill the following criteria: three or more unique peptides mapped to the protein or two unique peptides mapped to the protein but with at least 30% coverage. The relative protein amounts were calculated and the fold changes in *zmndf6* mutant relative to the wild type were presented.

Metabolite profiling

Maize and rice samples were harvested from the same stages of plants used for RNA-seq. Each biological replicate consisted of 4 leaf discs (diameter=8 mm) from one individual plant, and at least 6 biological replicates (6 plants from 3 different mutant lines) were prepared for measurement. For each biological replicate, 4 leaf discs (approximately 40 mg) were flash frozen (dropped into liquid nitrogen within 1 second after cutting) and ground in a tissue grinding machine, 30 Hz × 1 min, three times. The ground powder was mixed with 800 μL extraction buffer [methanol: chloroform = 7:3 (v/v), -20°C pre-cooled], shaken in the tissue grinding machine (30 Hz for 3 min), and the mixture was kept in -20°C for 3-4 h. The mixture was added with 560 μL cold distilled water, shaken in the tissue grinding machine (30 Hz for 5 min), and put back in -20°C for 10 min. The sample was centrifuged at 2200 g, for 10 min at 4°C, and the supernatant (about 800 μL) was transferred to a new tube and kept in -20°C. For a 2nd extraction, 800 μL of 50% methanol was added to the pellet and the tube was carefully vortexed for 15 s before put back in -20°C. After 30 min, it was centrifuged again at 2200 g, for 10 min at 4°C, and the supernatant (about 800 μL) was combined with last extraction. The total supernatant (about 1.6 mL) was filtered by 0.22 μm filter, and 5 μL were injected for HPLC-MS/MS analysis or for quality control.

Luna NH2 column (3μm, 100mm x 2mm, Phenomenex co. Ltd, USA) was used in liquid chromatography, and the separation was conducted with a gradient set of solution A (20 mM Ammonium acetate in 5% acetonitrile solution, adjusted to pH 9.5 with ammonia water) and solution B (acetonitrile): 0~1 min, 15% A and 85% B; 1~8 min, 70% A and 30% B; 8~22 min, 95% A and 5% B; 22~25 min, 15% A and 85% B. Mass spectrometry analysis of the eluent was performed with QTRAP 6500+ (AB Sciex, co. Ltd, USA) in multi reaction monitoring (MRM) mode, parameters were referred from previous work (Tang *et al*., 2022), and data analysis was performed using Analyst®1.6 software.

Metabolites detected were identified by aligning the retention time to features of standard samples previous processed on the same platform (Tang *et al*., 2022). The relative amounts of each metabolite in different samples were calculated by the chromatographic peak areas, and the changes of the metabolites relative to the averaged values of the wild type were presented. The data presentation was adopted from Li *et al*., 2020.

Accession numbers

Accession numbers for the genes measured by qRT–PCR are as follows: *ZmCA*(Zm00001eb037940), *ZmPEPC*(Zm00001eb383680), *ZmNADP-MDH* (Zm00001eb038930),*ZmPPDK*(Zm00001eb287770),*ZmME*(Zm00001eb121470),*ZmRbcS*(Zm00001eb197410),*ZmRbcL1*(Zm00001eb440790),*ZmRbcL2*(Zm00001eb187470), and *OsActin*(Os03g0718100).

Results

Construction of NDF6 and NDHU subunit deficient mutants in maize and rice

Chloroplast NDH is structurally divided into five subcomplexes: A, B, M(membrane), L(lumen) and ED(electron donor) **(Fig. S1a)**. Subcomplex B is composed of five subunits (PnsB1-5), and is specific to chloroplast NDH (Shikanai, 2015; Ma *et al*., 2021). By data mining, we found that the expression of *NDF6* (gene assigned as *PnsB4* recently) and *NDHU* (NDHU belongs to subcomplex ED) in maize BS cells was higher than in M cells, and higher in maize leaves than in rice leaves (Li *et al*., 2010; Wang *et al*., 2014) **(Table S1; Fig. S1b)**. In addition, their up-regulation amplitude in maize leaves relative to rice leaves was much higher than that of *NDHN* and *NDHO*, which had been reported in maize deletion mutants (Peterson *et al*., 2016), while *PGR5* and *PGRL1* were not highly expressed in maize leaves compared to rice leaves **(Table S1; Fig. S1b)**. To dissect and compare the significance of

NDH-mediated CET in C_4 and C_3 photosynthesis, we generated maize and rice loss of function mutants of NDF6 and NDHU subunits using CRISPR-Cas9 technology.

For maize *ndh* mutants, two sgRNAs each were designed for the near 5'-terminal sequences of the first exons of *ZmNDF6* and *ZmNDHU* genes to construct gene editing vectors. Seven *ZmNDF6* edited and 5 *ZmNDHU* edited maize plants were obtained, and materials with 49bp, 51bp and 54bp homozygous deletions (starting at 16bp after ATG) in *ZmNDF6* gene were named *zmndf6-1*, *zmndf6-2* and *zmndf6-3*, respectively. Two homozygous mutation types in *ZmNDHU*, *zmndhu-1* and *zmndhu-2* were identified **(Fig. S2a, c)**.

For *ndh* mutants in rice, a single sgRNA near 5' end of the third exon of the *OsNDF6* gene and the first exon of the *OsNDHU* gene was designed respectively to construct gene editing vectors. Twelve *OsNDF6* edited rice plants were obtained, including 3 *osndf6* homozygous lines with 3bp or 10bp deletions or a single base insertion. They were named *osndf6-1*, *osndf6-2* and *osndf6-3*, respectively. Seven *OsNDHU* edited materials were sequenced but all T0 plants were found to be heterozygous. After segregation, we identified homozygous *osndhu* mutants with single A-base insertion or 163bp deletion and named them *osndhu-1* and *osndhu-2* respectively **(Fig. S2b, d)**.

Retarded growth of *ndf6* and *ndhu* mutants in maize but not in rice

After 30 days culture of T1 plants in a phytotron, the growth of *zmndf6* and *zmndhu* mutants was retarded compared with that of the wild type KN5585 **(Fig. 1a)**. Leaf chlorophyll contents and plant height of *zmndf6* and *zmndhu* mutants were significantly lower than those of the wild type **(Fig. 1b)**. The yellowish leaf colour of T1 plants was more obvious after 30 days in field greenhouse than in the phytotron **(Fig. S3)**. Rice *osndf6* and *osndhu* mutants showed no considerable difference in growth, chlorophyll content, and plant

414 height compared with their wild type ZH11 **(Fig. 1c, d)**.

415 Post-illumination increase of chlorophyll fluorescence is used to indicate
416 the operation of CET. When the driving force of LET via PSII is absent, NDH
417 complex mediated electrons from the receptor side of PSI can flow back to
418 reduce the inter-system PQ pool, causing a recovery in PSII chlorophyll
419 fluorescence level (Asada *et al.*, 1993; Mano *et al.*, 1995; Mi *et al.*, 1995).
420 Compared with the wild type, the post-illumination increase of chlorophyll
421 fluorescence disappeared in *zmndf6* and *zmndhu* mutants, demonstrating that
422 the activity of CET was inhibited **(Fig. 2a)**. In addition, the decline of the
423 chlorophyll fluorescence induction curve under actinic light was slower in the
424 mutants than that in wild type, indicating a state of over-reduction of electron
425 transport chain **(Fig. S4)**. Far-red light induces an increase in 810-830 nm
426 absorption (representing oxidation of P700), and a decrease in light absorption
427 after far-red light (representing reduction of $P700^{+}$) reflects the rate of CET
428 around PSI (Maxwell and Biggins, 1976; Mi *et al.*, 1992; Asada *et al.*, 1992).
429 The dark reduction rate of $P700^{+}$ in *zmndf6* and *zmndhu* mutants was
430 significantly lower than that of the wild type **(Fig. 2b)**, indicating the partial
431 inactivation of CET. Thus, a series of maize ZmNDF6 and ZmNDHU functional
432 deletion mutants were successfully obtained.

433 To evaluate whether CET in rice NDH deficient mutants was affected, we
434 measured the chlorophyll fluorescence and $P700^{+}$ reduction in *osndf6* and
435 *osndhu* leaves. Compared with the wild type, the post-illumination increase of
436 chlorophyll fluorescence was decreased in *osndf6* and *osndhu* mutants **(Fig.**
437 **2a)**, but unlike in maize, there was no major difference in the descending
438 phase of chlorophyll fluorescence under actinic light. The $P700^{+}$ reduction rate
439 of *osndf6* and *osndhu* mutants decreased to different degrees compared with
440 that of the wild type **(Fig. 2b)**. These results show that the activity of the CET
441 pathway was also impeded in the rice NDH deficient mutants.
442

Photosynthetic CO_2 assimilation was severely impaired in maize but not in rice NDH deficient mutants

To further explore whether and to what extent the photosynthetic activity of NDH deficient C_4 and C_3 plants was affected, we tested the CO_2 response curve (A/Ci), electron transfer rate (ETR), non-photochemical quenching (NPQ) and other photosynthetic parameters of the maize and rice mutants. It was found that the initial slopes of the A/Ci curve, as well as the level of steady state photosynthetic rate, were clearly lower in maize *zmndf6* and *zmndhu* mutants than those in wild type **(Fig. 3a, b)**. The levels of ETR and NPQ in *zmndf6* and *zmndhu* mutants were also notably lower than those in wild type **(Fig. S5a, b)**.

Different from the variation observed in maize *zmndf6* and *zmndhu* mutants, the initial slopes of the A/Ci curve, and the level of steady state photosynthetic rate, were not notably different in rice *osndf6* and *osndhu* mutants from those in wild type (except that the A/Ci curve of *osndf6* mutants appeared lower than wild type) **(Fig. 3c, d)**. Measurements of ETR and NPQ also showed no considerable difference between the rice *ndh* mutants and the wild type **(Fig. S5c, d)**.

In addition, it is noteworthy that the stomatal conductance (gs) of *zmndf6* and *zmndhu* mutants was not different or lower than that of the wild type, while intercellular CO_2 concentration (Ci) was increased, especially in the 3 strains of *zmndf6* mutant **(Fig. 3e, f)**. This implies that CO_2 assimilation was inhibited but it was not due to stomatal limitation. Changes of stomatal conductance and intercellular CO_2 concentration in the rice *ndh* mutants were not obvious **(Fig. 3g, h)**.

Decreased photosynthetic proteins and abnormal chloroplast ultrastructure in maize *ndf6* and *ndhu* mutants

To test whether the decreased photosynthesis of maize *ndh* mutants was

related to decreased protein levels in the leaves, we compared the changes of protein components in PSI, PSII, cytochrome b6f, NDH, ATP synthase, and Rubisco between the mutants and the wild type. As expected, western blot analysis showed that NDF6 subunit was almost undetectable in the leaves of the *zmndf6* **(Fig. 4a)**, and NDHU subunit in *zmndhu* could barely be detected **(Fig. 4b)**. The protein levels of NDHH, NDHS, and NDHO subunits were also decreased in the maize *ndh* mutants **(Fig. 4a, b)**. The decrease of these subunits likely affected the amount and assembly of the NDH-PSI super complex as well, as reflected by blue-native gel and a 2nd-dimension electrophoresis **(Fig. 4e, f)**. By detecting the subunits of PSI and PSII, we found that the protein level of PsaA but not PsaD subunit tends to be lower in *zmndf6*, while PsaD but not PsaA subunit tends to be lower in *zmndhu* than in wild type. The protein level of PsbA (D1) was lower in both *zmndf6* and *zmndhu* than in wild type, while the PetA subunit of cytochrome b6f complex (PetA was found decreased in BS proteome, **Fig. S7a**) and the AtpB subunit of ATP synthase were not notably different from that of the wild type. Importantly, we found that the protein levels of RbcL in *zmndf6* (although RbcL is barely decreased in *zmndf6-1*) and *zmndhu* were notably decreased **(Fig. 4a, b)**, which supports the decreased CO_2 assimilation activity of the maize NDH deficient mutants **(Fig. 3a, b)**.

Protein levels of NDH subunits tested were also much decreased in the rice *osndf6* and *osndhu* mutants, but in contrast to the situation in the maize mutants, protein levels related to PSI, PSI, cytochrome b6f, ATP synthase, and Rubisco were not notably changed compared with the wild type (only PsaD and PsaA showed a slight downward trend) **(Fig. 4c, d)**. The differential changes in protein levels support the observation that photosynthetic electron transport, CO_2 assimilation rates, and plant growth were compromised in maize but not rice *ndh* mutants, although CET activity was decreased in both.

To explore the relationship between the amount and integrity of NDH-PSI

protein complex and thylakoid lamellar structure of maize BS chloroplasts, transmission electron microscopy was performed on maize wild type and *zmndf6* leaf samples. Compared with the wild type, non-stacking stromal thylakoid tended to be less assembled in the BS chloroplasts of maize *zmndf6* mutant, and areas with intermittent distribution or even absence of lamellae were observed **(Fig. 5a, b, e, f)**. For M cell chloroplasts, the thickness of the grana thylakoid was decreased and the grana lamellae were not well aligned in the *zmndf6* mutant compared with the wild type **(Fig. 5c, d, g, h)**. In addition, the starch granule accumulation of BS cells was lower in the mutant than in the wild type **(Fig. 5a, b, e, f)**. In accordance with this, starch staining by I_2-KI in leaf paraffin sections showed that both the amount of starch synthesized early in the day and the accumulation late in the day were lower in the *ndh* mutants than that in the wild type **(Fig. 5j)**. The reduction in starch content is most probably caused by the decreased photosynthetic activity in maize *ndh* mutants **(Fig. 3)**.

Up-regulated gene expression of Calvin-Benson cycle and cyclic electron transport in maize *ndh* mutants

In order to explore how and to what extent photosynthesis and other related pathways were affected at the transcriptional level, RNA sequencing was carried out on leaves of maize and rice NDH deficient mutants. We systematically analysed the differential expression of photosynthesis related functional genes, which were converted from a complete list of maize photosynthetic proteins demonstrated in Friso *et al.*, 2010. Generally, gene expression in the two maize *ndh* mutants behaved differently from that in the rice *ndh* mutants, with transcript abundance linked with CET pathway and Calvin-Benson cycle mostly higher **(Fig. 6, for details with gene lists see Fig. S6)**.

The expression of genes involved in LET, such as PSII, PSI, cytochrome

b6f, and ATP synthase showed varied changes in the maize *zmndf6* and *zmndhu* mutants. Among this, the expression of genes encoding LHCII-1.4 and LHCII-1.5 were drastically and uniformly down-regulated (up to 8.6 fold) in the two maize mutants. Those up-regulated include genes encoding OEC23-like oxygen-evolving complex, PsbS, and Rieske domain protein **(Figs 6, S6a)**. As for the components related to CET, the *zmndf6* and *zmndhu* mutants displayed down-regulation of *NDF6* and *NDHU,* as expected, and lower transcript level of an extra gene of *NDF2*. Apart from that, the expression of PGR5 or other NDH-pathway associated nuclear genes showed consistent trends of up-regulation, including *PTOX* (plastid terminal oxidase) and *PIFI* (post-illumination chlorophyll fluorescence increase) **(Figs 6, S6b)**. In the rice *osndf6* and *osndhu* mutants, the expression of genes involved in LET showed consistent down-regulation. Interestingly, although most transcripts related to CET were down-regulated in the two rice mutants, *PTOX* and *PIFI* that are involved in chloroplast respiration were up-regulated **(Figs 6, S6a, b)**.

In maize *zmndf6* and *zmndhu* mutants, the expression of genes related to Calvin-Benson cycle and photorespiration was comprehensively up-regulated, especially for Rubisco activase (RCA) and Fructose-bisphosphate aldolase-2 (SFBA-2). One distinct exception is the markable down-regulation of FBPase in both maize *ndh* mutants **(Figs 6, S6c)**. Correspondingly, the expression of genes related to starch biosynthesis also showed extensive up-regulation **(Fig. S6d)**. In rice *osndf6* and *osndhu* mutants, there was no consistent up-regulation of Calvin-Benson cycle or photorespiration-related gene expression, indeed there was a tendency for down-regulation **(Fig. S6c)**. It should be noted that in line with increased levels Calvin-Benson cycle related transcripts in *osndf6* than in *osndhu* mutants, the expression of starch biosynthesis-related genes was also different between the two mutants **(Fig. S6d)**. This indicated the existence of intrinsic or physiological differences between rice *osndf6* and *osndhu* mutants.

559

560 **Effects of NDH deficiency on the BS specific C_4 genes and ROS**
561 **accumulation**

562 Transcriptome analysis revealed that a deficient NDH pathway resulted in
563 distinct changes in maize compared to rice at the level of gene expression. As
564 chloroplast signals participate in nucleus-plastid communication (Surpin *et al.*,
565 2002; Baier and Dietz, 2005), the redox changes within chloroplasts caused by
566 lack of NDH **(Fig. S4)** may be one of the reasons for these gene expression
567 changes. Specifically, we measured the gene expression of C_4 enzymes in the
568 maize *zmndf6* and *zmndhu* mutants by qRT-PCR. Consistent with the
569 transcriptomic data, the expression of major genes (more abundant in
570 transcripts) encoding BS cell localized ME, RbcS, and RbcL1 were
571 up-regulated in *zmndf6* mutants, by 2.27, 4.26, and 4.35 fold, respectively. In
572 contrast, the major gene expression of M cell localized PEPC, MDH, and
573 PPDK did not markedly change or even decreased in the *zmndf6* mutants **(Fig.**
574 **6c)**. Similarly, an increased expression of BS specific C_4 genes was observed
575 in the *zmndhu* mutant.

576 To verify the redox changes in the chloroplasts of maize *ndh* mutants, we
577 detected the accumulation of reactive oxygen species (ROS) in the BS and M
578 cells by 3,3-Diaminobenzidine (DAB) staining **(Fig. 5i)**. DAB reacts with H_2O_2
579 to generate brown polymers that are stable in most solutions. With DAB
580 uptaken by leaves, H_2O_2 can be localized *in situ* and at a subcellular level
581 (Thordal-Christensen *et al.*, 1997). Signal was densely exhibited in the BS
582 chloroplasts of *zmndf6* and *zmndhu* mutants, and brown staining was also
583 visible in the neighbouring M chloroplasts. In the wild type, overall staining
584 intensity was much less than that in the *ndh* mutants **(Fig. 5i)**. These results
585 indicate a remarkable increase in ROS accumulation in both BS and M cells
586 when NDH is deficient in maize leaves, while in wild type leaves a balanced
587 redox state contributes to lower ROS level. Less PSII and high NDH-CET is

588 probably beneficial to prevention of ROS in the BS cells.

589

590 **Effects of NDH deficiency on the BS cell proteome**

591 In order to further explore the effect of NDH deficiency specific in maize BS
592 cells, we conducted a proteomic analysis by comparing the isolated BS cells of
593 WT and *zmndf6* mutant. First of all, we found that contents of many NDH
594 subunits (including NDHU, NDHM, NDHN, PnsB1, and PnsL2) significantly
595 decreased, while contents of PGR5 and PGRL1 remained less changed,
596 reassuring that the mutation of ZmNDF6 has reduced the abundance of NDH
597 complex in maize BS cells **(Fig. 6d)**. The contents of BS specific C4 enzyme
598 NADP-ME and Rubisco activase (especially RCA2) increased, although the
599 contents of Rubisco subunits did not change (different from whole leaf Western
600 blot, the similar amount of Rubisco here may be related to its highly enriched
601 proportion in the BS of both WT and *zmndf6* mutant). Interestingly, consistent
602 with the gene expression data, SFBA content enhanced whereas FBPase
603 content declined. Further analysis of the proteins involved in starch synthesis
604 revealed that beta-amylase (BAM3, BAM9), which is responsible for
605 hydrolyzing starch to maltose, was significantly upregulated **(Fig. 6d; Fig.**
606 **S7b)**.

607 On the other hand, proteins associated with PSI complex were
608 significantly less in *zmndf6* mutant. Since PSI and NDH form super-complex,
609 the deficiency of NDH complex in *zmndf6* mutant seems to also affect the
610 abundance of PSI proteins. Components of ATP synthase appeared to be
611 stable, while components related to Cytb6/f complex (PetA, PetD, and PetC for
612 example) decreased. It is worth noting that STN7 and STN8 (involved in state
613 transition), as well as FNR1 and FNR3 (responsible for electron transport
614 between NADPH and Ferredoxin), were significantly up-regulated in *zmndf6*
615 BS cells, indicative of remarkable changes in distribution of light energy and
616 electron flow **(Fig. S7a)**. Analysis of the changes of proteins related to redox

regulation showed significant downregulation of Thioredoxin and Peroxidase, indicated that loss of ZmNDF6 seriously affected the redox environment in maize BS cells **(Fig. S7b)**.

Impaired NDH-CET caused critical changes in photosynthetic carbon metabolism in maize

The measured changes in photosynthesis, gene expression, and protein contents suggested that NDH deficiency had different impacts on CO_2 assimilation in maize and rice. We therefore examined how NDH influenced photosynthetic metabolism using the maize and rice leaves for metabolic analysis. Metabolic profiles of the maize *zmndf6* and *zmndhu* mutants were found to be relatively consistent with each other, with obvious common up-regulated or down-regulated components, certifying the reliability of our biological samples and the effects caused by *NDH* mutations **(Fig. 7a)**. Specifically, metabolites involved in the Calvin-Benson cycle in maize *ndh* mutants were generally decreased compared with the wild type, except for RuBP and FBP, which accumulated significantly **(Fig. 7a, d)**. The accumulation of RuBP was consistent with the decrease in protein content of Rubisco large subunit **(Fig. 4a, b)** and the increase of intercellular CO_2 concentration **(Fig. 3e, f)** in the mutants. In contrast to the decrease of most metabolites in the Calvin-Benson cycle, metabolites at earlier steps of photorespiration, such as 2PG, Glyco, Glx and Gly, increased in maize *ndh* mutants **(Fig. 7a, f)**, indicating an increase in photorespiration, which was consistent with a previous report (Peterson *et al.*, 2016).

Extending the viewpoint to C_4 metabolic cycle, we found that PEP, Pyr and Asp decreased to varying degrees, whereas malate increased in both *zmndf6* and *zmndhu* mutants **(Fig. 7a, e)**, which correlates with the increased gene expression and protein content of NADP-ME **(Fig. 6)**. Changes in malate probably also led to the accumulation of Fum, which interconverts with it in the

tricarboxylic acid cycle (TCA cycle), while the levels of its upstream metabolites, such as CIT, ICIT, αKG, and Succ, decreased **(Fig. 7g)**. In addition, we have calculated the ATP/ADP, NADH/NAD and NADPH/NADP ratios, and the results indicate that the ATP/ADP ratio may not change, whereas the NADPH/NADP ratio is strongly increased in the two *ndh* mutants of maize **(Fig. 7h)**. The ratios are important because several NADPH participated C_4 reactions are reversible, including the NADP-MDH and NADP-ME mediated reactions in the M and BS chloroplasts respectively. It should be mentioned that many of the metabolites are compartmentalized with a sub-pool being involved in C_4 metabolism, the case of malate for example. It is possible that the changes are also among some other pool and not only in the pool that is involved in C_4 metabolism.

The metabolic profiles of rice *osndf6* and *osndhu* mutants displayed more variable fluctuations, and an overall trend of decreased contents **(Fig. 7b, c)**. This metabolic variability may be related to the different gene expression patterns of the Calvin-Benson cycle between the two rice mutants **(Figs 6, S6c)**. On the other hand, while the levels of NADPH and adenylate in maize *ndh* mutants increased, the levels of them in rice *ndh* mutants appeared decreased **(Fig. 7b, c)**. These results support the remarkable difference in CO_2 assimilation status observed between the maize and rice NDH deficient mutants.

Discussion

To maintain an efficient Calvin-Benson cycle in the framework of the C_4 pathway, it is necessary to dynamically balance the metabolism of both substance and energy. In this study, we show that NDH-mediated CET plays a crucial role in this process. The necessity and continuity of this regulation may be more prominent in C_4 BS cells of maize, which provide a relatively special redox environment due to imported malate and NADPH. **Fig. 8** provides a

summarized interpretation.

NDH cyclic electron transport balances C_4 metabolism and carbon flow in addition to ATP supply

Using NDH deficient mutants of maize and rice for comparison, we found that the metabolite and energy flows were effectively disrupted for C_4 but not for C_3 photosynthesis. Previous studies found that the direct electron donor of NDH was ferredoxin (Fd), and electrons were transferred between NADPH and Fd through ferridoxin-$NADP^+$ reductase (FNR) (Ifuku *et al.*, 2011; Peltier *et al.*, 2016). Since NADPH is coupled to decarboxylation of the malate entering into BS cells, NDH may play a special role in maintaining the electron flow of PSI (the dominant component of BS chloroplasts), regeneration of $NADP^+$, and the input of malate along the concentration gradient. This study demonstrates that both NADPH and malate tend to accumulate in maize *zmndf6* and *zmndhu* mutants, which is different from the situation in equivalent mutants in rice **(Fig. 7)**. The accumulation of malate and NADPH could be caused by the impaired NADPH turnover, and further caused by the decreased demand from Calvin-Benson cycle, as reflected by the accumulation of RuBP and lower levels of many other intermediates **(Fig. 7)** in maize *ndh* mutants. In contrast, photorespiration was favoured, leading to more production of 2-phosphoglyolate, and elevated levels of other intermediates in the first part of the pathway, such as glycolate and glyoxylate.

It is worth to note that the distinct down-regulation of gene expression for FBPase, together with the up-regulation of gene expression for fructose-bisphosphate aldolase (SFBA), echoes well with the FBP accumulation in maize *ndh* mutants **(Fig. S6c)**, indicating an important site specific regulation which is pending to be resolved. The accumulation of FBP also indicated an effect of the NDH pathway on rate-limiting steps of the Calvin-Benson cycle, and its involvement in the feedback regulation of CET, as

the FBPase deficient mutant (*hcef1*) was reported to specifically upregulate NDH and increase CEF (Livingston *et al.*, 2010a, 2010b). Embden-Meyerhof-Parnas pathway (EMP, also named glycolysis) is the primary step of cellular respiration and the universal pathway of glucose degradation. Pentose phosphate pathway (PPP) is an alternative route for carbohydrate degradation. As NADPH is generated in the G6P and 6GP dehydrogenization steps of the PPP pathway, and the PPP pathway connects to the EMP pathway via G6P **(Fig. 7g)**, whether the accumulation of FBP downstream of G6P in the EMP pathway was affected by NADPH accumulation is an open question, and FBP maybe also a hub for alternative carbon flow towards EMP and PPP pathway. Many EMP pathway and TCA cycle components decreased, with the exceptions of FBP, Fum, and Mal. Considering these pathways together, the contents of αKG and $NADP^+$ decreased, while the contents of 2PG and RuBP increased in maize *ndh* mutants. Since the two metabolite pairs of "αKG, $NADP^+$" and "2PG, RuBP", play active or inhibitory roles in the CO_2 concentration mechanism of cyanobacteria (Daley et al., 2012), it is possible that a similar regulatory role occurs in C_4 plants.

On another hand, NDH-mediated CET is believed to be a key source of ATP required by C_4 photosynthesis, especially in the BS cells of NADP-ME type C_4 plants. This view is supported by the ability of NDH-mediated CET to couple additional ATP synthesis, the observed higher NDH content in C_4 plants than in C_3 plants, and the NDH enrichment in cell types requiring additional ATP for CO_2 concentration (Takabayashi *et al.*, 2005; Ishikawa *et al.*, 2016b). The ATP/ADP ratio appeared not changed in *zmndf6* and *zmndhu mutants* compared with the wild type **(Fig. 7h)**. A possible explanation could be the decreased ATP consumption due to inhibited metabolic processes, although ATP supply was likely impaired in the maize *ndh* mutants.

NDH cyclic electron transport poises C_4 BS cell redox to regulate CO_2 assimilation

The Calvin–Benson cycle is a redox regulated process. Many enzymes related to CO_2 assimilation, including Glyceraldehyde-3-phosphate dehydrogenase (GAPDH), Phosphoribulokinase (PRK), Fructose-1,6-bisphosphatase (FBPase), Sedoheptulose-1,7-bisphosphatase (SBPase), NADP-dependent malatedehydrogenase (NADP-MDH), and Rubisco activase were known to be activated by the light through ferredoxin/thioredoxin-dependent reduction of regulatory disulfide bonds (Michelet et al., 2013). As BS chloroplasts have little PSII, disruption of NDH-CET may interfere with the provision of electrons for the reduction of ferredoxin and, hence, thioredoxin. The reduced thioredoxins are able to reduce regulatory disulfides and activate their target enzymes (Buchanan, 1991; Michelet et al., 2013). How and to what extent this is related to the interesting changes of Rubisco activase, FBPase, NADP-ME, beta-amylase and so forth in *zmndh* mutants, remain to be further examined. On the other hand, the accumulation of malate and NADPH in *zmndh* mutants is probably responsible for the over-reduced state of chloroplast stroma, and the obstructed status of electron transport chain **(Figs S4, S5)**. The increased ROS accumulation in the BS cells of *zmndf6* and *zmndhu* mutants **(Fig. 5i)** would be caused by the over-reduction, and this could negatively affect the content and activity of Rubisco, as well as Rubisco activase. The resultant inactivation of Calvin-Benson cycle in maize *ndh* mutants eventually leads to decrease of photosynthetic rate and the plant growth defects **(Figs 1, 3)**.

The decarboxylation of C_4 acids in the BS cells is a key step in C_4 photosynthesis. NADP-ME operation in the direction of decarboxylation is known to be hampered by high NADPH/NADP ratio, which has been recently highlighted by Andrea Brautigam (Brautigam et al., 2018), indicating that oxidized redox poise in the chloroplast stroma favors high velocity of decarboxylation. They summarized that BS chloroplasts achieve more

762 oxidized state via the consumption of NADPH by Calvin-Benson cycle and the
763 limited production of NADPH by abolishing PSII activity in BS cells. Here our
764 results suggest a 3rd driving force of BS-enriched NDH-CET by NADPH
765 turnover. In maize BS cells where malate is imported into and decarboxylated
766 to release NADPH, it is possible that NDH-CET is needed to poise the NADPH
767 level, so that its loss leads to the observed increase of the NADPH levels and
768 the NADPH/NADP ratio, which in turn restricts decarboxylation by NADP-ME,
769 leading to lower BS CO_2 concentration, lower pyruvate content, and over
770 accumulated malate level. The low BS CO_2 concentration would restrict the
771 Rubisco carboxylase reaction, together with the damage of Rubisco and
772 Rubisco activase by accumulated ROS, explaining the high RuBP and lower
773 levels of many other Calvin-Benson cycle intermediates.

774 As part of the early attempts to install C_4 pathway, C_4-specific NADP-ME
775 was over-expressed in rice, but it led to bleaching of leaf color and growth
776 hindrance, which resulted from enhanced photoinhibition due to an increase in
777 the level of NADPH inside the chloroplast (Tsuchida et al., 2001). The malate
778 and NADPH imbalance, pale green leaf, retarded growth, and ROS
779 accumulation observed in our maize NDH function deficient mutants, are
780 reminiscent of the effect of NADP-ME over-expression. The increased
781 transcript level and BS protein content of NADP-ME strongly backup this
782 scenario **(Fig. 6c, 6d)**. Therefore, a functional or enhanced operation of
783 NDH-CET may be prerequisite when considering re-construction of the C_4
784 cycle. In another hand, a recent work showed that high light stress led to more
785 rapid ROS accumulation in BS than in M cells of rice, and also of C_4 species
786 (Xiong et al., 2021). The NDH deficiency resulted redox imbalance specific in
787 maize BS cells should be responsible to their increased ROS level even under
788 normal light.

789

790 **Deficiency of NDH disrupts the coordination of gene expression and**

protein accumulation in C_4 plants

The compartmentalization of photosystems and C_4 enzymes between BS and M cells is essential for the operation of C_4 photosynthesis in maize. The regulatory mechanisms behind C_4 differentiation remain unclear, but they probably involve the coordination of nuclear and plastid genomes, or specific changes in the intracellular environment to control gene expression in C_4 leaves. Because of the abundance of the NDH complex in maize BS cells, and its important role discussed above, our maize *zmndf6* and *zmndhu* mutants can be viewed with cellular changes mainly in the BS. In particular, changes in the redox state of PQ pools in the chloroplast can affect nuclear gene expression through retrograde signal transduction (Foyer *et al.*, 2012). Our data showed that the gene expression of the BS cell-specific C_4 enzymes ME, RbcS, and RbcL1 were up-regulated remarkably, whereas the gene expression of M cell-specific enzymes PEPC, MDH and PPDK did not change or decreased in *zmndf6* mutants **(Fig. 6c)**. The BS specific protein contents of NADP-ME and Rubisco activase were consistently increased, but not the Rubisco subunits, which might be subject to more regulation or change on protein level.

With respect to cellular changes in M cells, Covshoff *et al.* identified a maize high chlorophyll fluorescence mutant (*hcf136*) with a PSII abnormality (Covshoff *et al.*, 2008). Cell type-specific gene expression analysis showed that, compared with the wild type, the expression of M cell specific genes was promoted while that of BS cells was decreased. The authors suggested that the change of gene expression in M cells was related to retrograde signals from plastid to nucleus, while the change of gene expression in BS cells was more likely a secondary response caused by decreased reducing power or metabolite input (Covshoff *et al.*, 2008). In another work, by studying the greening of *Cleome gynandra* leaves, combined with Norflurazon treatment, Burgess *et al.* pointed out that the regulation of C_4 gene expression is

considerably dependent on the chloroplasts, and light-induced activation of these genes is lost in damaged chloroplasts (Burgess *et al.*, 2016).

Interestingly, according to the transcriptome analysis, apart from the CRISPR targeted *NDF6* and *NDHU* genes, the expression of many other NDH pathway-associated nuclear genes, as well as *PGR5* and *PTOX*, showed various degrees of up-regulation **(Fig. S6b)** in maize *zmndf6* and *zmndhu* mutants. One possible trigger could be the increased ROS accumulation in these mutants, as Strand *et al.* found that treatment of leaves with H_2O_2 could improve the NDH complex-dependent CET activity (Strand *et al.*, 2015). It could be also partly attributed to the feedback signals, from the decreased protein levels of many NDH subunits. Equally remarkable, Calvin-Benson cycle related gene expression were comprehensively and consistently up-regulated in the two maize *ndh* mutants **(Fig. S6c)**. We suspect that these parallel changes of gene expression between CET and Calvin-Benson cycle are closely related or feedback affected by the changes of protein levels **(Figs 4, 6d)**, metabolic flows **(Fig. 7)**, or redox state. It could be also a projection of the intrinsic involvement of NDH pathway in the regulation of C_4 carbon metabolism. Studies on the genus Flaveria indicated that NDH increased during the evolution of C_4 pathway, especially during the transition stage from C_3-C_4 intermediate to C_4-like (Nakamura *et al.*, 2013), further suggesting that the function of NDH in NADP-ME C_4 plants may be more closely related to the regulation of carbon metabolism. However, it remains difficult to identify genetic regulators that systematically upregulate NDH expression.

In conclusion, as modelled in **Fig. 8**, we propose that NDH cyclic electron transport forms an indispensable regulatory circuit for the two-celled C_4 photosynthetic system in maize. The significance of the NDH pathway in C_4 plants can be attributed to both ATP supply and NADPH turnover, as well as the adjustment of malate flux and NADP-ME activity. The loss of NDH function

leads to metabolic, redox, and other regulatory imbalances, especially in BS cells, which then feedback to affect the coordination of photosynthetic gene expression and protein levels. Our study advances the functional understanding of NDH enrichment in maize BS cells, and hopefully will inspire fine tuning strategies to be re-considered towards engineering C_4 photosynthesis.

Acknowledgments

We thank Prof. Hualing Mi and Prof. Jane Langdale for critical comments on this work. We thank You Zhang and Luhuan Ye for helping with gas exchange, chlorophyll fluorescence, and P700 measurements; Zai Shi, Rui Zhang, and Yanfei Fan for other material and instrument assistance. We are grateful to Xiaoyan Gao, Zhiping Zhang, Jiqin Li, Wenli Hu, Shanshan Wang and Xiaoyan Xu for technical support on TEM and HPLC-MS; Chunguang Chen from ORIZYMES for antibody generation and Mi lab for gift of other antibodies; WIMI Biotechnology for maize and rice mutant generation. This research was funded by Strategic Priority Research Program (No. XDA24010203-2), the National Natural Science Foundation of China (No. 31970257), and a joint grant for international exchange from Royal Society and National Natural Science Foundation of China to Andrew J. Fleming and Peng Wang (No. 32011530166).

Author contributions

QZ and PW conceived the project; QZ performed most experiments, data analyses and produced the figures; ST analyzed the RNA-seq data; QT and GC provided essential help for metabolite measurement. QZ, YZ, AJF, XZ and PW interpreted the results, wrote, and revised the paper with input from all authors.

Data availability

The mRNA-seq datasets generated in this study have been deposited into the SRA database at NCBI under BioProject IDs PRJNA843342.

References

Alvarez CE, Detarsio E, Moreno S, Andreo CS, Drincovich MF. 2012. Functional characterization of residues involved in redox modulation of maize photosynthetic NADP-malic enzyme activity. *Plant Cell Physiol* 53(6):1144–53.

Asada K, Heber U, Schreiber U. 1992. Pool size of electrons that can be donated to P700+, as determined in intact leaves: donation to P700+ from stromal components via the intersystem chain. *Plant Cell Physiol* **33**: 927–932.

Asada K, Heber U, Schreiber U. 1993. Electron flow to the intersystem chain from stromal components and cyclic electron flow in maize chloroplasts, as detected in intact leaves by monitoring redox change of P700 and chlorophyll fluorescence. *Plant Cell Physiol* **34**: 39–50.

Baier M, Dietz KJ. 2005. Chloroplasts as source and target of cellular redox regulation: a discussion on chloroplast redox signals in the context of plant physiology. *J Exp Bot* **56**(416): 1449–1462.

Bauwe H, Hagemann M, Fernie AR. 2010. Photorespiration: players, partners and origin. *Trends Plant Sci* **15**: 330–336.

Bräutigam A, Kajala K, Wullenweber J, Sommer M, Gagneul D, Weber KL, Carr KM, Gowik U, Mass J, Lercher MJ, Westhoff P, Hibberd JM, Weber AP. 2011. An mRNA blueprint for C4 photosynthesis derived from comparative transcriptomics of closely related C3 and C4 species. *Plant Physiol* **155**(1): 142–156.

Bräutigam A, Schlüter U, Lundgren MR, Flachbart S, Ebenhöh O, Schönknecht G, Christin PA, Bleuler S, Droz JM, Osborne CP, Weber APM, Gowik U. 2018. Biochemical mechanisms driving rapid fluxes in C4 photosynthesis. *bioRxiv* preprint doi: https://doi.org/10.1101/387431

Buchanan, BB. 1991. Regulation of CO2 assimilation in oxygenicphotosynthesis: the ferredoxin/thioredoxin system. Perspective on its discovery, present status, and futuredevelopment. *Arch Biochem Biophys* 288, 1–9.doi:10.1016/0003-9861(91)90157-E

Burgess SJ, Granero-Moya I, Grangé-Guermente MJ, Boursnell C, Terry MJ, Hibberd JM. 2016. Ancestral light and chloroplast regulation form the foundations for C4 gene expression. *Nat Plants* **2**(11): 16161.

Burrows PA, Sazanov LA, Svab Z, Maliga P, Nixon PJ. 1998. Identification of a functional respiratory complex in chloroplasts through analysis of tobacco mutants containing disrupted plastid ndh genes. *EMBO J* **17**(4): 868–876.

Covshoff S, Majeran W, Liu P, Kolkman JM, van Wijk KJ, Brutnell TP. 2008. Deregulation of maize C4 photosynthetic development in a mesophyll cell-defective mutant. *Plant Physiol* **146**(4): 1469–1481.

Daley SM, Kappell AD, Carrick MJ, Burnap RL. 2012. Regulation of the cyanobacterial CO_2-concentrating mechanism involves internal sensing of NADP+ and α-ketogutarate levels by transcription factor CcmR. *PLoS One* **7**(7): e41286.

Darie CC, Biniossek ML, Winter V, Mutschler B, Haehnel W. 2005. Isolation and structural characterization of the Ndh complex from mesophyll and bundle sheath chloroplasts of Zea mays. *FEBS J* **272**(11): 2705–2716.

Darie CC, De Pascalis L, Mutschler B, Haehnel W. 2006. Studies of the Ndh complex and photosystem II from mesophyll and bundle sheath chloroplasts of the C4-type plant Zea mays. *J Plant Physiol* **163**(8): 800–808.

Drincovich MF, Casati P, Andreo CS. 2001. NADP-malic enzyme from plants: a ubiquitous enzyme involved in different metabolic pathways. *FEBS Lett* **490**: 1–6.

Endo T, Shikanai T, Takabayashi A, Asada K, Sato F. 1999. The role of chloroplastic NAD(P)H dehydrogenase in photoprotection. *FEBS Lett* **457**(1): 5–8.

Ermakova M, Danila FR, Furbank RT, von Caemmerer S. 2020. On the road to C4 rice: advances and perspectives. *Plant J* **101**(4):940–950.

Friso G, Majeran W, Huang M, Sun Q, van Wijk KJ. 2010. Reconstruction of metabolic pathways, protein expression, and homeostasis machineries across maize bundle sheath and mesophyll chloroplasts: large-scale quantitative proteomics using the first maize genome assembly. *Plant Physiol* **152**(3): 1219–1250.

Foyer CH, Neukermans J, Queval G, Noctor G, Harbinson J. 2012. Photosynthetic control of electron transport and the regulation of gene expression. *J Exp Bot* **63**(4): 1637–1661.

Furbank RT. 2017. Walking the C4 pathway: past, present, and future. *J Exp Bot* **68**(2): 4057–4066.

Horváth EM, Peter SO, Joët T, Rumeau D, Cournac L, Horváth GV, Kavanagh TA, Schäfer C, Peltier G, Medgyesy P. 2000. Targeted inactivation of the plastid ndhB gene in tobacco results in an enhanced sensitivity of photosynthesis to moderate stomatal closure. *Plant Physiol* **123**(4): 1337–1350.

Hughes TE, Langdale JA. 2020. SCARECROW gene function is required for photosynthetic development in maize. *Plant Direct* **4**(9): e00264.

Ifuku K, Endo T, Shikanai T, Aro EM. 2011. Structure of the chloroplast NADH dehydrogenase-like complex: nomenclature for nuclear-encoded subunits. *Plant Cell Physiol* **52**(9): 1560–1568.

Ishikawa N, Endo T, Sato F. 2008a. Electron transport activities of Arabidopsis thaliana mutants with impaired chloroplastic NAD(P)H

dehydrogenase. *J Plant Res* **121**(5): 521–526.

Ishikawa N, Takabayashi A, Noguchi K, Tazoe Y, Yamamoto H, von Caemmere, S, Sato F, Endo T. 2016a. NDH-Mediated Cyclic Electron Flow Around Photosystem I is Crucial for C4 Photosynthesis. *Plant Cell Physiol* **57**(10): 2020–2028.

Ishikawa N, Takabayashi A, Sato F, Endo T. 2016b. Accumulation of the components of cyclic electron flow around photosystem I in C4 plants, with respect to the requirements for ATP. *Photosynth Res* **129**(3): 261–277.

Ivanov B, Asada K, Edwards GE. 2007. Analysis of donors of electrons to photosystem I and cyclic electron flow by redox kinetics of P700 in chloroplasts of isolated bundle sheath strands of maize. *Photosynth Res* **92**(1): 65–74.

Johnson GN. 2011. Physiology of PSI cyclic electron transport in higher plants. *Biochim Biophys Acta* **1807**(3): 384–389.

Kouřil R, Strouhal O, Nosek L, Lenobel R, Chamrád I, Boekema EJ, Šebela M, Ilík P. 2014. Structural characterization of a plant photosystem I and NAD(P)H dehydrogenase supercomplex. *Plant J* **77**(4): 568–576.

Kubicki A, Funk E, Westhoff P, Steinmu¨ ller K. 1996. Differential expression of plastome-encoded ndh genes in mesophyll and bundle-sheath chloroplasts of the C4 plant Sorghum bicolor indicates that the complex I-homologous NAD(P)H-plastoquinone oxidoreductase is involved in cyclic electron transport. *Planta* **199**: 276–281.

Li P, Ponnala L, Gandotra N, Wang L, Si Y, Tausta SL, Kebrom TH, Provart N, Patel R, Myers CR, Reidel EJ, Turgeon R, Liu P, Sun Q, Nelson T, Brutnell TP. 2010. The developmental dynamics of the maize leaf transcriptome. *Nat Genet* **42**(12): 1060–1067.

Livingston AK, Cruz JA, Kohzuma K, Dhingra A, Kramer DM. 2010a. An Arabidopsis mutant with high cyclic electron flow around photosystem I (hcef) involving the NADPH dehydrogenase complex. *Plant Cell* **22**(1): 221–233.

Livingston AK, Kanazawa A, Cruz JA, Kramer DM. 2010b. Regulation of cyclic electron flow in C_3 plants: differential effects of limiting photosynthesis at ribulose-1,5-bisphosphate carboxylase/oxygenase and glyceraldehyde-3-phosphate dehydrogenase. *Plant Cell Environ* **33**(11): 1779–1788.

Li XG, Duan W, Meng QW, Zou Q, Zhao SJ. 2004. The function of chloroplastic NAD(P)H dehydrogenase in tobacco during chilling stress under low irradiance. *Plant Cell Physiol* **45**(1): 103–108.

Li X, Wang P, Li J, Wei S, Yan Y, Yang J, Zhao M, Langdale JA, Zhou W. 2020. Maize GOLDEN2-LIKE genes enhance biomass and grain yields in rice by improving photosynthesis and reducing photoinhibition. *Commun Biol* **3**(1):151.

Long BM, Rae BD, Rolland V, Förster B, Price GD. 2016. Cyanobacterial

CO_2-concentrating mechanism components: function and prospects for plant metabolic engineering. *Curr Opin Plant Biol* 31:1–8.

Majeran W, van Wijk KJ. 2009. Cell-type-specific differentiation of chloroplasts in C4 plants. *Trends Plant Sci* **14**(2): 100–109.

Majeran W, Zybailov B, Ytterberg AJ, Dunsmore J, Sun Q, van Wijk KJ. 2008. Consequences of C4 differentiation for chloroplast membrane proteomes in maize mesophyll and bundle sheath cells. *Mol Cell Proteomics* **7**(9): 1609–1638.

Ma M, Liu Y, Bai C, Yong JWH. 2021. The Significance of Chloroplast NAD(P)H Dehydrogenase Complex and Its Dependent Cyclic Electron Transport in Photosynthesis. *Front Plant Sci* **12**: 661863.

Mano J, Miyake C, Schreiber U, Asada K. 1995. Photoactivation of the electron flow from NADPH to plastoquinone in spinach chloroplasts. *Plant Cell Physiol* **36**: 1589–1598.

Maxwell PC, Biggins J. 1976. Role of cyclic electron transport in photosynthesis as measured by the photoinduced turnover of P700 in vivo. *Biochemistry* **15**(18): 3975–3981.

Michelet L, Zaffagnini M, Morisse S, Sparla F, Pérez-Pérez ME, Francia F, Danon A, Marchand CH, Fermani S, Trost P, Lemaire SD. 2013. Redox regulation of the Calvin-Benson cycle: something old, something new. *Front Plant Sci* **25**;4:470. doi: 10.3389/fpls.2013.00470.

Mi H, Endo T, Asada K. 1992. Donation of electrons to the intersystem chain in the cyanobacterium Synechococcus sp. PCC7002 as determined by the reduction of P700+. *Plant Cell Physiol* **33**: 1099–1105.

Mi H, Endo T, Ogawa T, Asada K. 1995. Thylakoid membrane-bound, NADPH-specific pyridine nucleotide dehydrogenase complex mediates cyclic electron transport in the cyanobacterium Synechocystis PCC6803. *Plant Cell Physiol* **36**: 661–668.

Munekage YN, Eymery F, Rumeau D, Cuiné S, Oguri M, Nakamura N, Yokota A, Genty B, Peltier G. 2010. Elevated expression of PGR5 and NDH-H in bundle sheath chloroplasts in C4 flaveria species. *Plant Cell Physiol* **51**(4): 664–668.

Nakamura N, Iwano M, Havaux M, Yokota A, Munekage YN. 2013. Promotion of cyclic electron transport around photosystem I during the evolution of NADP-malic enzyme-type C4 photosynthesis in the genus Flaveria. *New Phytol* **199**(3): 832–842.

Ogawa T, Kobayashi K, Taniguchi YY, Shikanai T, Nakamura N, Yokota A, Munekage YN. 2023. Two cyclic electron flows around photosystem I differentially participate in C4 photosynthesis. *Plant Physiol* **27**:kiad032. doi: 10.1093/plphys/kiad032.

Peltier G, Aro EM, Shikanai T. 2016. NDH-1 and NDH-2 Plastoquinone Reductases in Oxygenic Photosynthesis. Annu. Rev. *Plant Biol* **67**: 55–80.

Peng L, Fukao Y, Fujiwara M, Takami T, Shikanai T. 2009. Efficient operation of NAD(P)H dehydrogenase requires supercomplex formation

with photosystem I via minor LHCI in Arabidopsis. *Plant Cell* **21**(11): 3623–3640.

Peng L, Shikanai T. 2011. Supercomplex formation with photosystem I is required for the stabilization of the chloroplast NADH dehydrogenase-like complex in Arabidopsis. *Plant Physiol* **155**(4): 1629–1639.

Peng L, Shimizu H, Shikanai T. 2008. The chloroplast NAD(P)H dehydrogenase complex interacts with photosystem I in Arabidopsis. *J Biol Chem* **283**(50): 34873–34879.

Peterson RB, Schultes NP, McHale NA, Zelitch I. 2016. Evidence for a Role for NAD(P)H Dehydrogenase in Concentration of CO_2 in the Bundle Sheath Cell of Zea mays. *Plant Physiol* **171**(1): 125–138.

Price GD, Pengelly JJ, Forster B, Du J, Whitney SM, von Caemmerer S, Badger MR, Howitt SM, Evans JR. 2013. The cyanobacterial CCM as a source of genes for improving photosynthetic CO_2 fixation in crop species. *J Exp Bot* **64**(3):753–68.

Raines CA. 2011. Increasing photosynthetic carbon assimilation in C3plants to improve crop yield: current and future strategies. *Plant Physiol* **155**: 36–42.

Shikanai T. 2014. Central role of cyclic electron transport around photosystem I in the regulation of photosynthesis. *Curr Opin Biotechnol* **26**: 25–30.

Shikanai T. 2015. Chloroplast NDH: A different enzyme with a structure similar to that of respiratory NADH dehydrogenase. *Biochim Biophys Acta* **1857**(7): 1015–1022.

Strand DD, Fishe, N, Kramer DM. 2017. The higher plant plastid NAD(P)H dehydrogenase-like complex (NDH) is a high efficiency proton pump that increases ATP production by cyclic electron flow. *J Biol Chem* **292**(28): 11850–11860.

Strand DD, Livingston AK, Satoh-Cruz M, Froehlich JE, Maurino VG, Kramer, DM. 2015. Activation of cyclic electron flow by hydrogen peroxide in vivo. *Proc Natl Acad Sci U S A* **112**(17): 5539–5544.

Suorsa M. 2015. Cyclic electron flow provides acclimatory plasticity for the photosynthetic machinery under various environmental conditions and developmental stages. *Front Plant Sci* **6**: 800.

Surpin M, Larkin RM, Chory J. 2002. Signal transduction between the chloroplast and the nucleus. *Plant Cell* **14**(Suppl): S327–S338.

Takabayashi A, Kishine M, Asada K, Endo T, Sato F. 2005. Differential use of two cyclic electron flows around photosystem I for driving CO_2-concentration mechanism in C4 photosynthesis. *Proc Natl Acad Sci U S A* **102**(46): 16898–16903.

Tang QM, Huang YH, Ni XX, Ming-Ju Amy Lyu, Chen GY, Rowan Sage, Zhu XG. 2022. Increased α-ketoglutarate as a missing link from the C3-C4 intermediate state to C4 photosynthesis in the genus Flaveria. *bioRxiv* 2022.06.01.494409 ; doi: https://doi.org/10.1101/2022.06.01.494409

Thordal-Christensen H, Zhang Z, Wei Y, Collinge DB. 1997. Subcellular localization of H_2O_2 in plants: H_2O_2 accumulation in papillae and hypersensitive response during the barley-powdery mildew interaction. *Plant J* **11**: 1187–1194.

Tsuchida H, Tamai T, Fukayama H, Agarie S, Nomura M, Onodera H, Ono K, Nishizawa Y, Lee BH, Hirose S, Toki S, Ku MS, Matsuoka M, Miyao M. 2001. High level expression of C4-specific NADP-malic enzyme in leaves and impairment of photoautotrophic growth in a C3 plant, rice. *Plant Cell Physiol* **42**(2): 138–145.

Turkan I, Uzilday B, Dietz KJ, Bräutigam A, Ozgur R. 2018. Reactive oxygen species and redox regulation in mesophyll and bundle sheath cells of C4 plants. *J Exp Bot* **69**(14): 3321–3331.

von Caemmerer S, Ghannoum O, Furbank RT. 2017. C4 photosynthesis: 50 years of discovery and innovation. *J Exp Bot* **68**(2): 97–102.

Wang L, Czedik-Eysenberg A, Mertz RA, Si Y, Tohge T, Nunes-Nesi A, Arrivault S, Dedow LK, Bryant DW, Zhou W, Xu J, Weissmann S, Studer A, Li P, Zhang C, LaRue T, Shao Y, Ding Z, Sun Q, Patel RV, Turgeon R, Zhu X, Provart NJ, Mockler TC, Fernie AR, Stitt M, Liu P, Brutnell TP. 2014. Comparative analyses of C_4 and C_3 photosynthesis in developing leaves of maize and rice. *Nat Biotechnol* **32**(11): 1158–1165.

Wang P, Duan W, Takabayashi A, Endo T, Shikanai T, Ye JY, Mi H. 2006. Chloroplastic NAD(P)H dehydrogenase in tobacco leaves functions in alleviation of oxidative damage caused by temperature stress. *Plant Physiol* **141**(2): 465–474.

Xiong H, Hua L, Reyna-Llorens I, Shi Y, Chen KM, Smirnoff N, Kromdijk J, Hibberd JM. 2021. Photosynthesis-independent production of reactive oxygen species in the rice bundle sheath during high light is mediated by NADPH oxidase. *Proc Natl Acad Sci U S A* **118**(25): e2022702118. doi: 10.1073/pnas.2022702118.

Yadav KN, Semchonok DA, Nosek L, Kouřil R, Fucile G, Boekema EJ, Eichacker LA. 2017. Supercomplexes of plant photosystem I with cytochrome b6f, light-harvesting complex II and NDH. *Biochim Biophys Acta Bioenerg* **1858**(1): 12–20.

Yamori W, Sakata N, Suzuki Y, Shikanai T, Makino A. 2011. Cyclic electron flow around photosystem I via chloroplast NAD(P)H dehydrogenase (NDH) complex performs a significant physiological role during photosynthesis and plant growth at low temperature in rice. *Plant J* **68**(6): 966–976.

Yamori W, Shikanai T. 2016. Physiological Functions of Cyclic Electron Transport Around Photosystem I in Sustaining Photosynthesis and Plant Growth. *Annu Rev Plant Biol* **67**: 81–106.

Zhou H, Akçay E, Helliker BR. 2019. Estimating C4 photosynthesis parameters by fitting intensive A/Ci curves. *Photosynth Res* **141**(2):181–194.

Supporting Information

Fig. S1 Comparison of the transcript levels of cyclic electron transport related components in maize and rice leaf gradients.

Fig. S2 Mutation of NDH genes in maize and rice with CRISPR-Cas9 technology.

Fig. S3 The phenotypes of maize *zmndf6* and *zmndhu* mutants growing in the field greenhouse.

Fig. S4 Induction kinetics and post-illumination increase in chlorophyll fluorescence in maize plants.

Fig. S5 Photosynthetic light reaction parameters in WT and *ndh* mutants.

Fig. S6 Transcriptome analysis of WT and *ndh* mutant leaves.

Table S1 Comparison of the BS/M ratio (mRNA or protein) of selected cyclic electron transport related components in maize.

Dataset S1 Transcriptome data of maize *zmndf6* and *zmndhu* mutants

Dataset S2 Transcriptome data of rice *osndf6* and *osndhu* mutants

Dataset S3 Expression of photosynthetic genes in maize and rice *ndh* mutants

Dataset S4 BS cell proteomics of maize WT and *zmndf6* mutant

Dataset S5 Metabolite analysis of maize and rice *ndh* mutants

Dataset S6 Summary of statistics

Dataset S7 Summary of primers

Figure Legends

Fig. 1 Altered growth phenotype in maize but not in rice *ndh* mutants

(a) Maize plants of WT(KN5585) and *ndh* mutants 30 days after planting. **(b)** Comparisons of chlorophyll content and plant height between WT and *ndh* mutants. Data are mean ± SE (n = 6 biological replicates for chlorophyll content and plant height). **(c)** Rice plants of WT(ZH11) and *ndh* mutants 60 days after planting. **(d)** Comparisons of chlorophyll content and plant height between WT and *ndh* mutants. Data are mean ± SE (n = 12 and 8 biological replicates for chlorophyll content and plant height respectively). *$P < 0.05$, **P

< 0.01 compared with WT according to Student's *t* test. WT* indicates the wild type used in a different batch together with *zmndhu* mutants, and ZH11* indicates the wild type used in a different batch together with *osndhu* mutants, due to timing and availability of transgenic materials.

Fig. 2 PSI cyclic electron flow was decreased in both maize and rice *ndh* mutants

(a) Measurement of NDH cyclic electron transport activity, which was detected as a transient increase in Chl fluorescence (surrounded by a box) after turning off the AL. **(b)** The re-reduction of $P700^+$ occurred after turning off the FR light, and comparison of the initial rates of $P700^+$ re-reduction between WT and *ndh* mutants was calculated. Curves were normalized to the maximum P700 oxidation level. Data are mean ± SE (n = 4 biological replicates). **P* < 0.05, ***P* < 0.01 compared with WT according to Student's *t* test. WT* indicates the wild type used in a different batch together with *zmndhu* mutants, and ZH11* indicates the wild type used in a different batch together with *osndhu* mutants, due to timing and availability of transgenic materials.

Fig. 3 CO_2 assimilation was severely inhibited in maize but not in rice *ndh* mutants

(a-d) CO_2 response curve of net photosynthetic assimilation rate (A/Ci) measured at 1200 μmol photons m^{-2} s^{-1} and 28 °C. (n = 3 biological replicates). **(e-h)** Stomatal conductance and intercellular CO_2 concentration (Ci) measured at 28 °C and 400 μmol CO_2 mol^{-1}. Data are mean ± SE (n = 3 biological replicates). **P* < 0.05, ***P* < 0.01 compared with WT according to Student's *t* test. WT* indicates the wild type used in a different batch together with *zmndhu* mutants, and ZH11* indicates the wild type used in a different batch together with *osndhu* mutants, due to timing and availability of transgenic materials.

Fig. 4 Immunoblot and BN-PAGE analysis reveals decreased amounts of photosynthetic proteins in maize *ndh* mutants

The changes of selected protein components of PSI, PSII, NDH, Cytb6f, ATP synthase and Rubisco between WT and the mutants leaves. **(a)** Proteins in maize KN5585 and *zmndf6* mutants. **(b)** Proteins in maize KN5585 and *zmndhu* mutants. **(c)** Proteins in rice ZH11 and *osndf6* mutants. **(d)** Proteins in rice ZH11 and *osndhu* mutants. **(e)** Thylakoid membrane protein complexes isolated from WT, *zmndf6* and *zmndhu* were solubilized and separated by BN-PAGE (5-12%). High molecular weight green bands specific to WT are indicated. **(f)** Thylakoid membrane protein complexes separated by BN-PAGE were subjected to 2nd dimension SDS-PAGE (12.5%), and the proteins were immunodetected with specific antibodies against NDHS, and NDHH, respectively. WT* indicates the maize wild type used in a different batch together with *zmndhu* mutants, and ZH11* indicates the rice wild type used in a different batch together with *osndhu* mutants, due to timing and availability of transgenic materials.

Fig. 5 Abnormal chloroplast structure and accumulation of ROS and starch in maize *ndh* mutant leaves

(a-h) Abnormal thylakoid ultrastructure of BS and M chloroplasts in maize *zmndf6* mutant. Transmission electron micrographs of BS chloroplast in WT **(a, b)**, M chloroplast in WT **(c, d)**, BS chloroplast in *zmndf6* **(e, f)**, and M chloroplast in *zmndf6* **(g, h)** are shown. “S” indicates starch granule. White triangles point to the broken ends of stromal thylakoid.

(i) DAB stained transections showing over-production of ROS in the BS cells of maize *zmndf6* and *zmndhu* mutants. Brown signals were densely visible in the BS cells of *zmndf6* and *zmndhu* mutants, but not in those of the wild type. Lower panel images (scale bar = 5 μm) are enlarged from indicated area of the upper panel images (scale bar = 20 μm).

(j) Light micrographs of transections showing less starch granules in maize *zmndf6* and *zmndhu* mutant leaves. Accumulation of starch grains in maize leaves at 7am and 7pm visualized by I_2–KI (iodine in potassium iodide solution) staining. Scale bar = 20 μm.

Fig. 6 Changes of gene expression and BS cell protein content in maize *ndh* mutants

(a) Heatmap shows differentially expressed genes in *ndh* mutants relative to their wild types (See **Fig. S6** for the heatmap with gene list). The significantly changed genes are assigned with numbers that link to names of encoded proteins in (b). The data represents mean value of 3 biological replicates. **(b)** Names of proteins encoded by significantly changed genes from (a). **(c)** RT-PCR validation showing increased transcript accumulation of BS but not M specific C_4 genes in maize *ndh* mutants. *CA*, Carbonic anhydrase; *PEPC*, Phosphoenolpyruvate carboxylase; *NADP-MDH*, NADP malate dehydrogenase; *PPDK*, Pyruvate phosphate dikinase; *ME*, Malic enzyme; *RbcS*, Rubisco small subunit; *RbcL1*, Rubisco large subunit 1; *RbcL2*, Rubisco large subunit 2. **(d)** Changes of BS cell specific CET pathway and CO_2 assimilation related protein contents. Comparisons were made between WT and *zmndf6* mutant according to quantitative values from BS cell proteomics. Data are mean ± SE (n = 3 biological replicates). $*P < 0.05$, $**P < 0.01$ compared with WT according to Student's *t* test.

Fig. 7 Loss of NDH-CET in maize leads to disturbance of key photosynthetic metabolites

(a) Relative abundance (log2-transformed fold changes) of photosynthetic metabolites in maize *zmndf6* and *zmndhu* mutants. WT: The mean of log2-fold changes of 4 WT (KN5585) values relative to their average. S1-S4: Fold changes of mutant values relative to the average value of WT. **(b, c)** Relative

abundance (log2-transformed fold changes) of photosynthetic metabolites in rice *osndf6* and *osndhu* mutants. ZH11: The mean of log2-fold changes of 6 WT (ZH11) values relative to their average. S1-S6: Fold changes of mutant values relative to the average value of WT. **(d-g)** Schematic diagrams showing key metabolites in **(d)** Calvin-Benson cycle (adapted from Figure 20-12, Biochemistry, sixth Edition, 2007, W.H. Freeman and Company), **(e)** C_4 metabolic cycle (the dotted arrows pointing from PEP through OAA to Asp indicate the likely reduced activity of this pathway in the *ndh* mutants), **(f)** photorespiration pathway, and **(g)** EMP, PPP pathways, and TCA cycle of maize *ndh* mutants. Heatmap arrays derived from *zmndf6* (upper row) and *zmndhu* (lower row) are listed on the side of corresponding metabolites. EMP pathway, Embden-Meyerhof-Parnas pathway, also known as glycolysis. PPP pathway, pentose phosphate pathway. TCA cycle, tricarboxylic acid cycle. **(h)** Ratios of NADPH/NADP, NADH/NAD, and ATP/ADP. Data are mean ± SE (n = 3 biological replicates). **P* < 0.05, ***P* < 0.01 compared with WT according to Student's *t* test.

Metabolite names showed in this figure are as follows: PGA (3-phosphoglyceric acid), DPGA (1,3-bisphosphoglyceric acid), FBP (Fructose 1,6-bisphosphate), GAP/DHAP(3-phosphoglyceraldehyde/Dihydroxyacetone), F6P (Fructose 6-phosphate), E4P (Erythrose 4-phosphate), S7P (Sedoheptulose 7-phosphate), PenP (Pentose phosphate, mixed of Ribose 5-phosphate, Xylulose 5-phosphate and Ribulose 5-phosphate), RuBP (Ribulose 1,5-bisphosphate), G6P/G1P (Glucose 6-phosphate/Glucose 1-phosphate), ADPG (Adenosine diphosphate glucose), UDPG (Uracil-diphosphate glucose), Sucrose (Sucrose), 2PG (Phosphoglycolic acid), Glyco (Glycolic acid), Glx (Glyoxylic acid), Gly (Glycine), Ser (Serine), Hpyr (Hydroxypyruvic acid), Glyce (Glyceric acid), aKG (α-Ketoglutaric acid), Gln (Glutamine), Glu (Glutamate), OAA (Oxaloacetic acid), Mal (Malic acid), Pyr

(Pyruvate), PEP (Phosphoenol pyruvate), Asp (Aspartate), Ala (Alanine), CIT (Citric acid), ICIT (Isocitric acid), Succ (Succinic acid), Fum (Fumaric acid), NAD (Nicotinamide adenine dinucleotide), NADH (Nicotinamide adenine dinucleotide reduced), NADP (Nicotinamide adenine dinucleotide phosphate), NADPH (Nicotinamide adenine dinucleotide phosphate reduced), ADP (Adenosine diphosphate), and ATP (Adenosine triphosphate).

Fig. 8 Schematic summary of the significance of NDH mediated cyclic electron transport in maize C_4 photosynthesis

(a) In the BS cells of wild type maize, malate is imported from M cells and mainly decarboxylated by NADP-ME, to release CO_2 and couple NADPH generation. CO_2 and NADPH is used in the Calvin-Benson cycle. Some of the NADPH may be involved in maintaining PSI-CET through the enriched NDH complex (bold red arrows compared to the thin red arrows in M cells), thus forming electron flows from malate to NADPH, from NADPH to PQ (via FNR, Fd, and NDH), and from PQ to PSI (through PC) or H_2O (through PTOX), as there is almost no PSII-LET in the BS cells. Note: Maize BS cells have low levels of PSII, but we are not showing BS PSII in this diagram to save place and emphasize the enrichment of PSI; the electron flow from NADPH via FNR to Fd is reversible, while we have made the arrow single way for easier understanding; NDF6 (PnsB4) belongs to subcomplex B in orange colour.
The process may be directly coupled with the CO_2 pump, during which $NADP^+$ is regenerated, ATP production is coupled, the input of malate along the concentration gradient continues, and Calvin-Benson cycle operates to fix CO_2. It should be noted that 3PGA/triose-P shuttle is also important for delivery of ATP and NADPH to the BS cells, but is not presented due to tight schematic layout. ROS generation preferentially occurs in the M cells.

(b) For a general comparison with wild type, in the BS cells of maize *ndh*

mutants, PSI-CET is inhibited (thin grey arrows), with malate and NADPH accumulate (colored red), leading to redox imbalance, decreased CO_2 fixation, increased ROS accumulation, and increased photorespiration.

Since malate continues to be imported into maize BS cells and releases NADPH, the enriched NDH in BS cells functions to balance NADPH turnover, PSI electron flow, and Calvin-Benson cycle, apart from ATP supplement. Calvin-Benson cycle was inhibited in maize *ndh* mutants as reflected by the decrease of many metabolites but specific accumulation of RuBP and FBP. In addition, as combined effects of malate import and NDH deficiency, BS cells of maize *ndh* mutants suffered from an over-reduced condition. The altered redox status and metabolites flow should have disturbed the cellular environment, and casts effects on gene expression and protein accumulation patterns.

Fig. 1

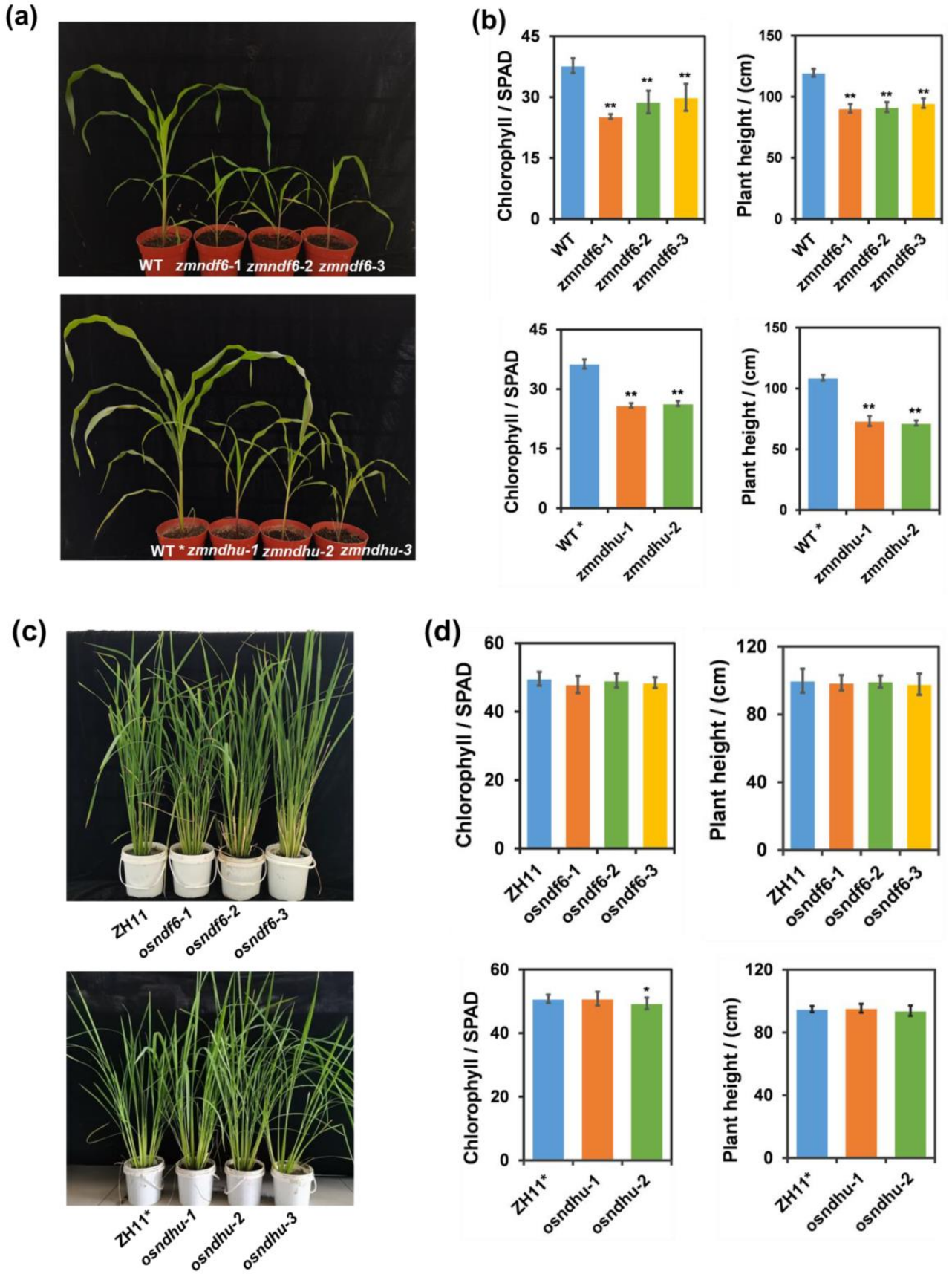

Fig. 2

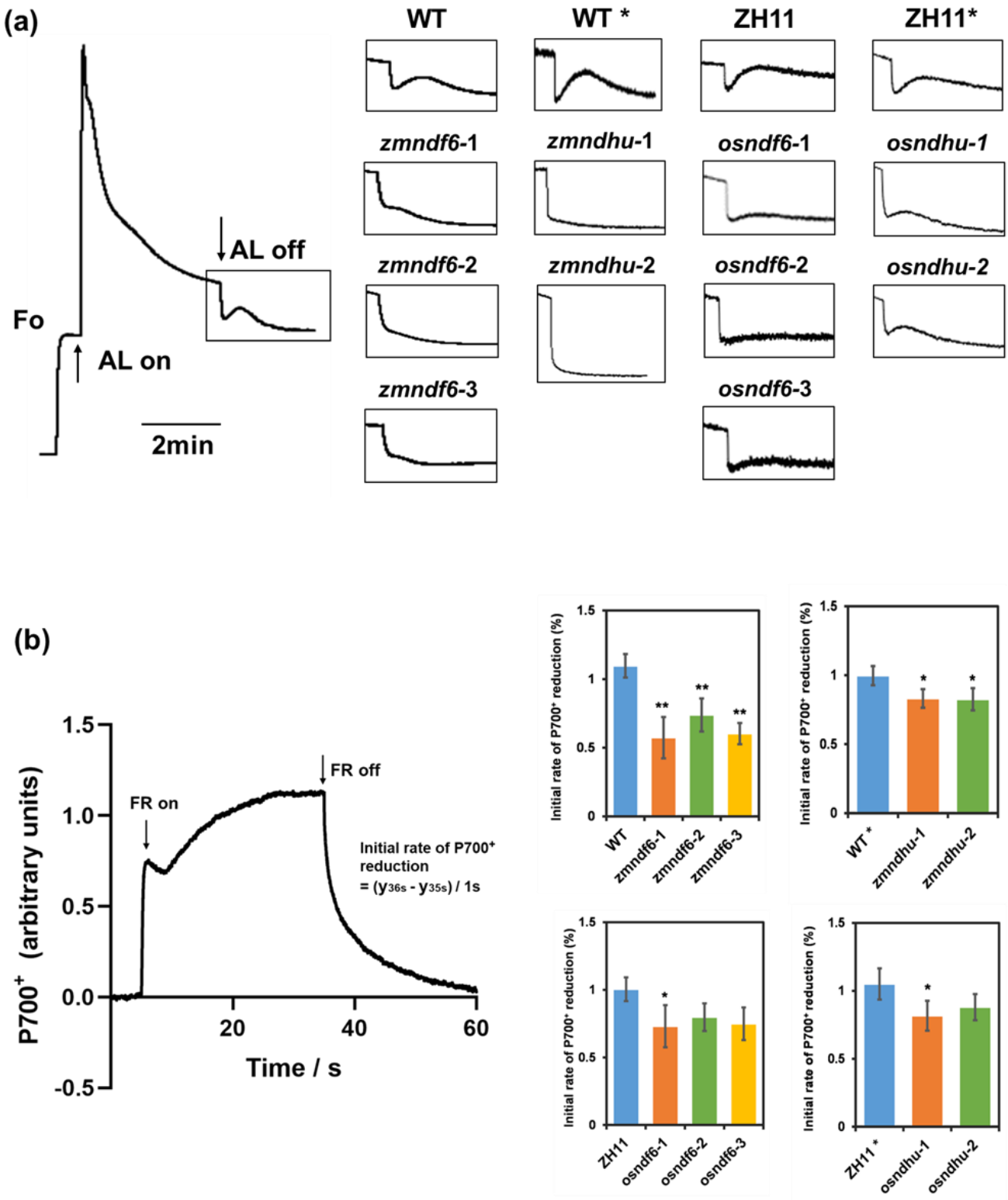

Fig. 3

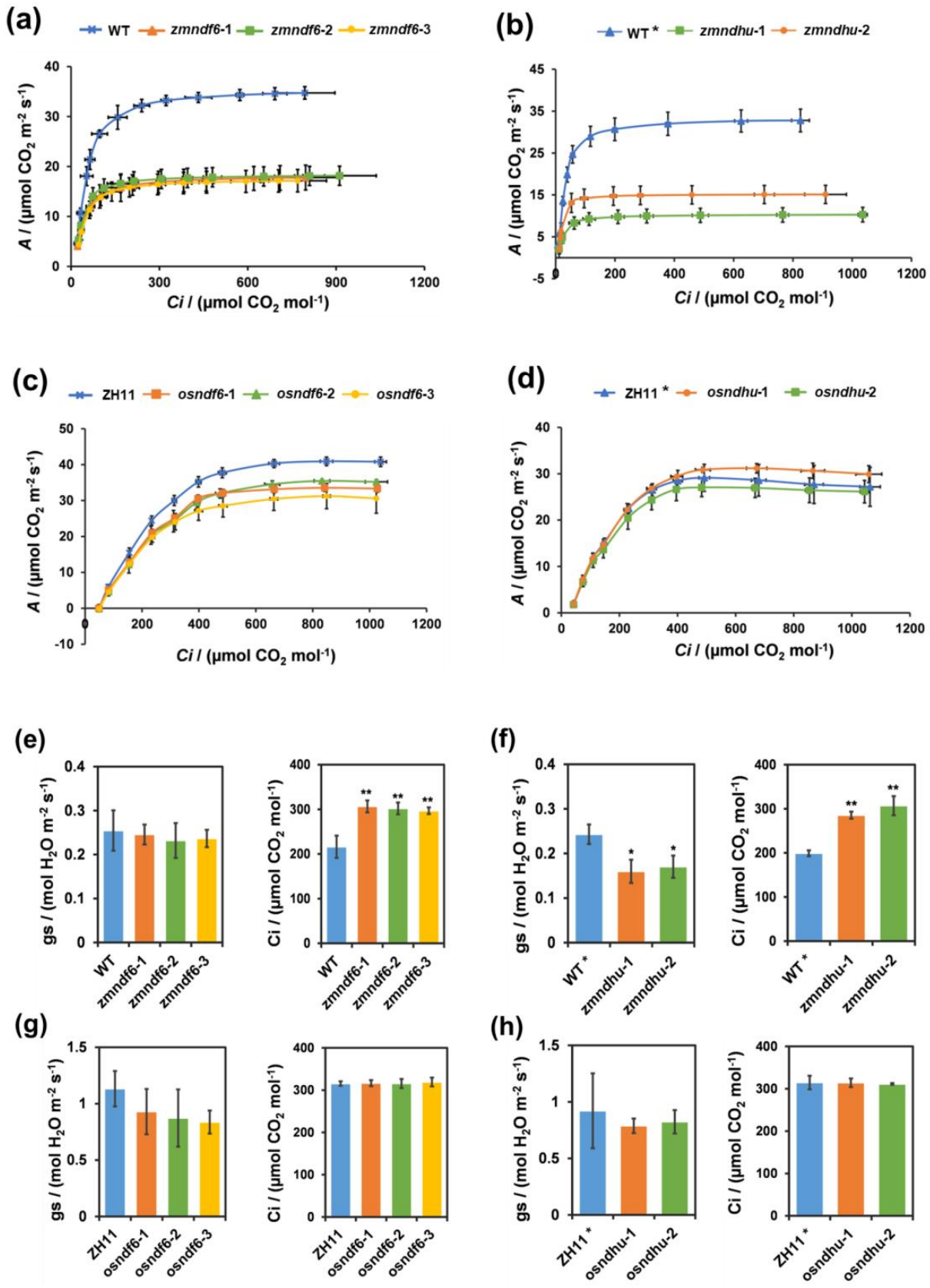

Fig. 4

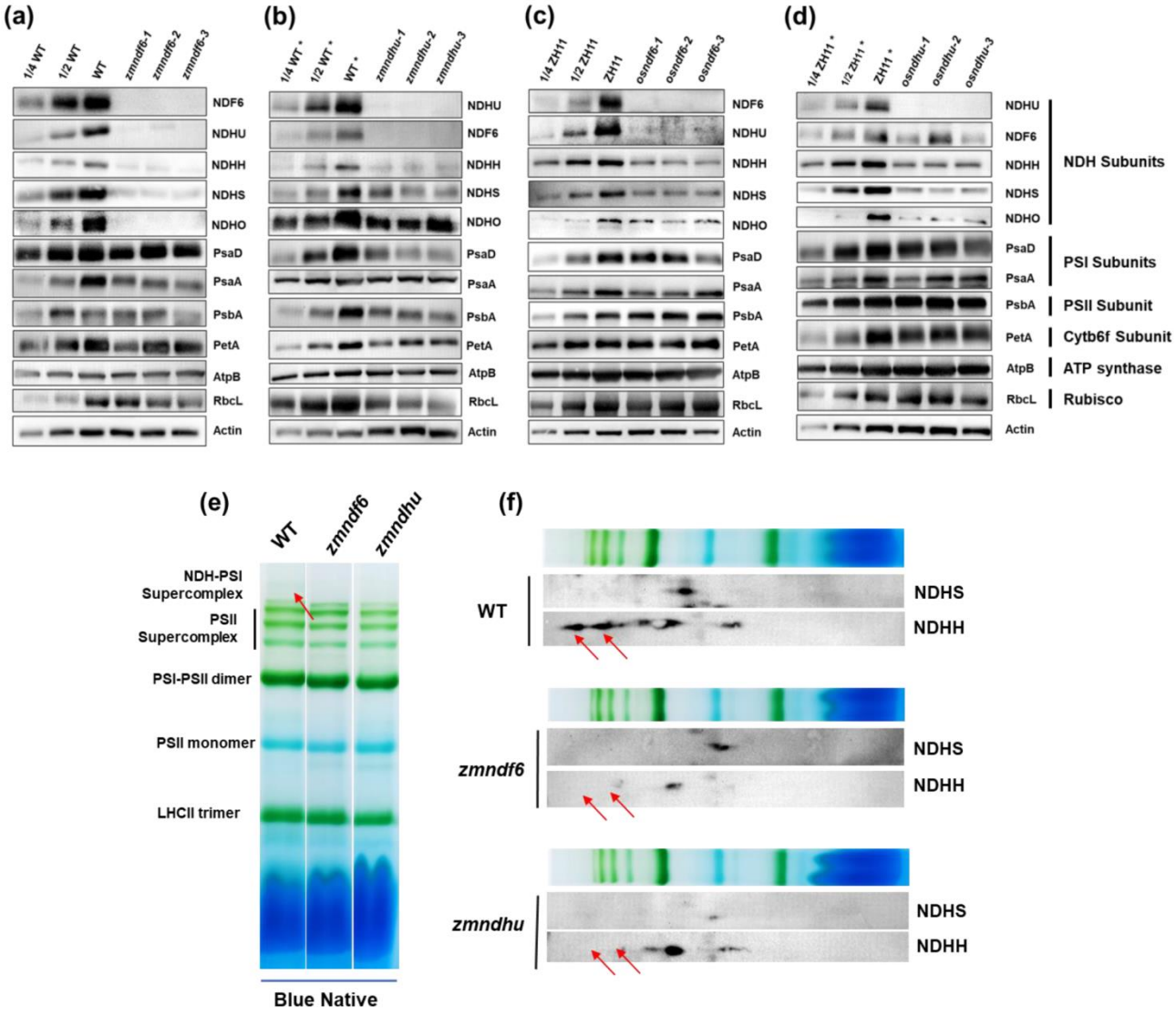

Fig. 5

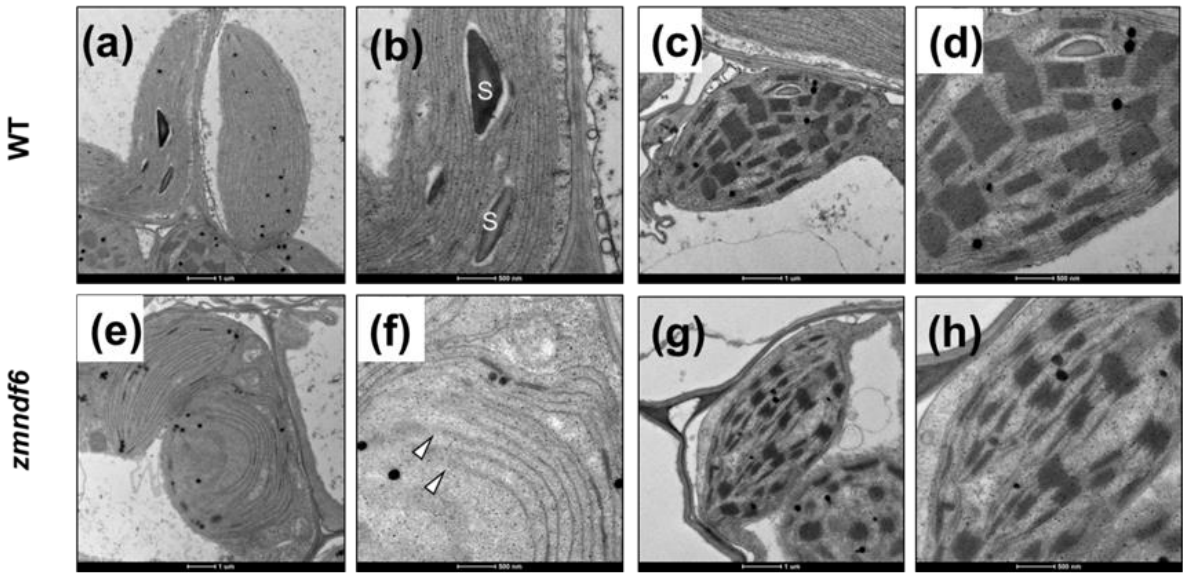

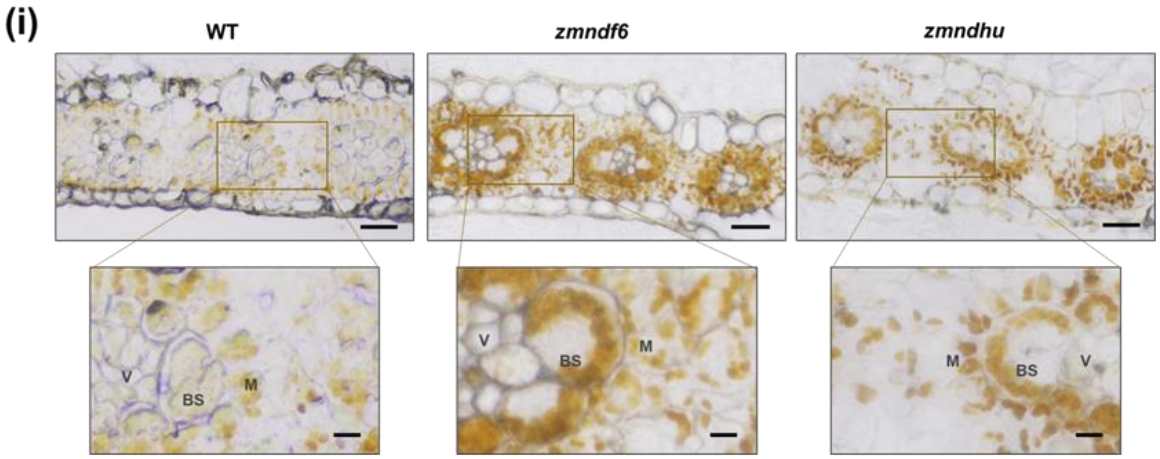

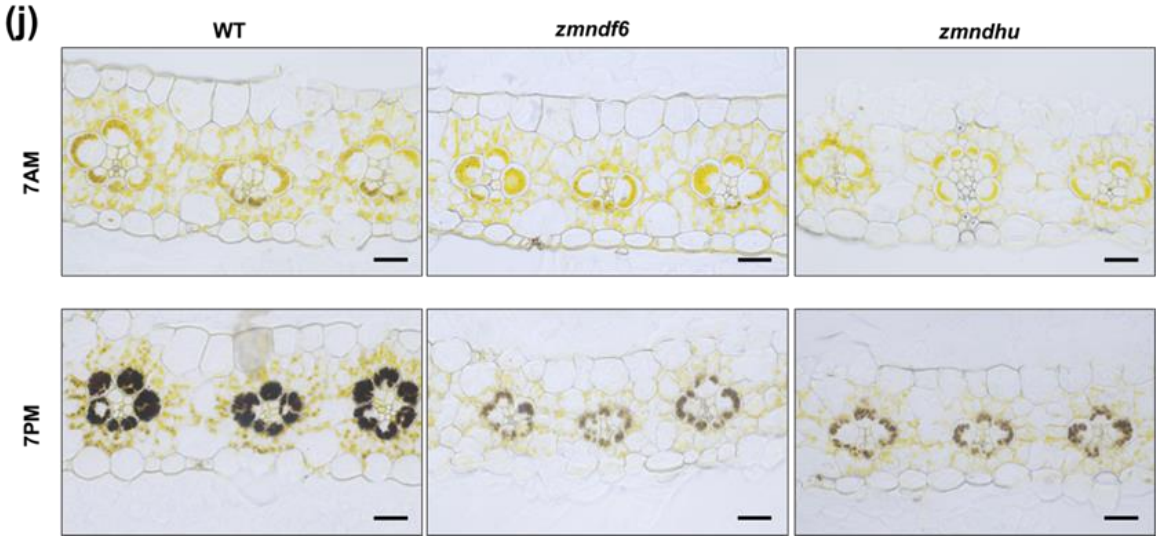

Fig. 6

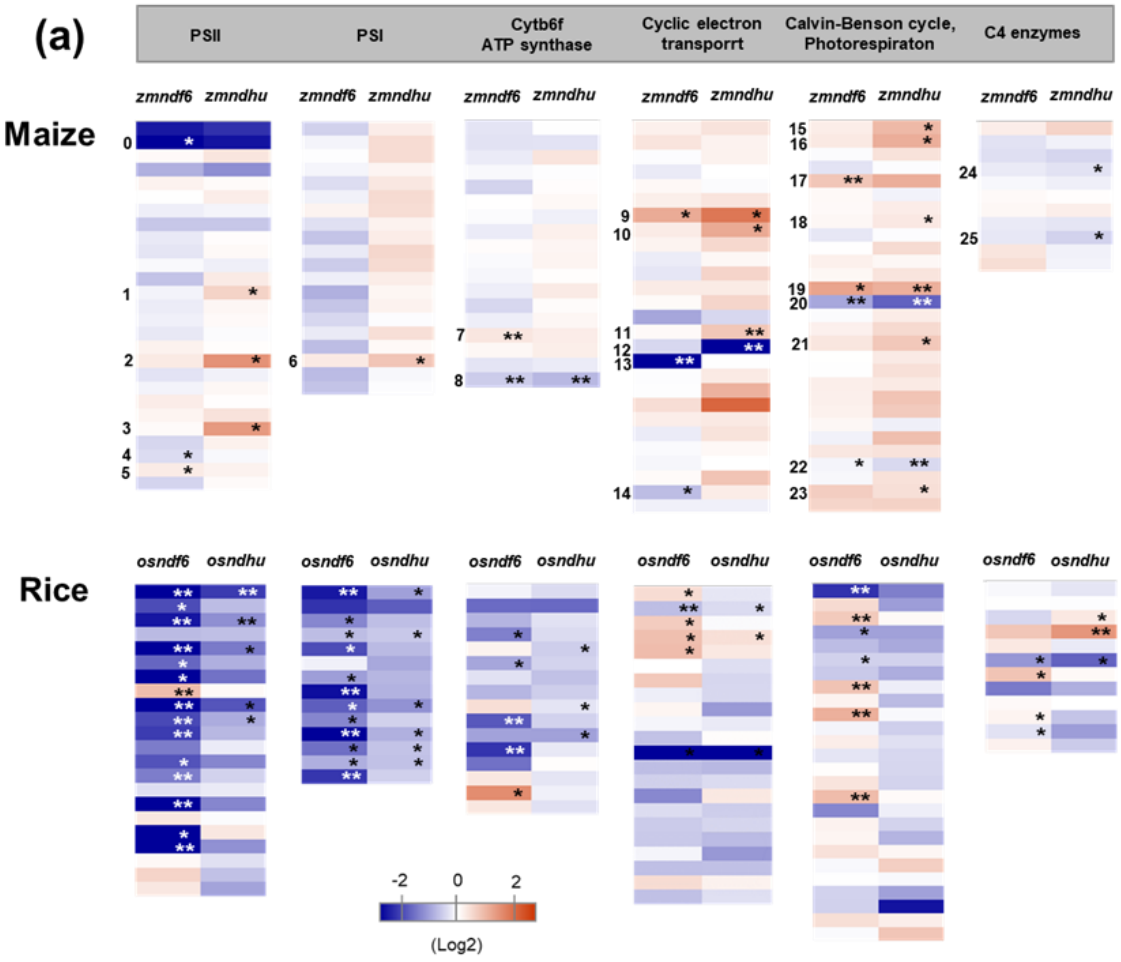

(b)

	Name		Name
0	LHCII-1.4 and 1.5 families	13	NDH F6 (PnsB4)
1	PSII Lumen Tat ITP -1	14	CRR6
2	OEC23-like-1	15	RBCS-4-2
3	OEC23-like-6 Tat ITP TP21.5	16	RBCS-4-1
4	psbR	17	RCA
5	psbS	18	PGK-1 (M-enriched)
6	psaL	19	SFBA-2
7	Rieske [2Fe-2S] domain protein	20	FBPase
8	FNR-1	21	SBPase
9	PIFI-1	22	PGP
10	PIFI-2	23	CAT1
11	PnsB3	24	PEPC
12	NDH U	25	CA2

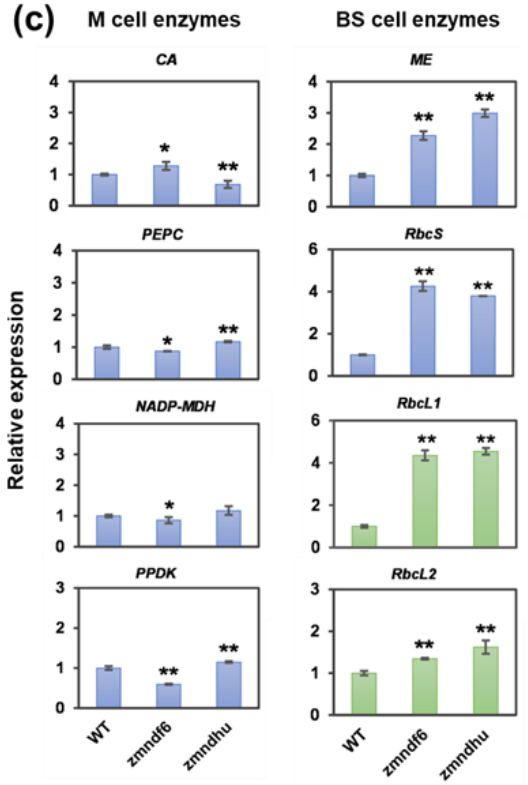

Fig. 6

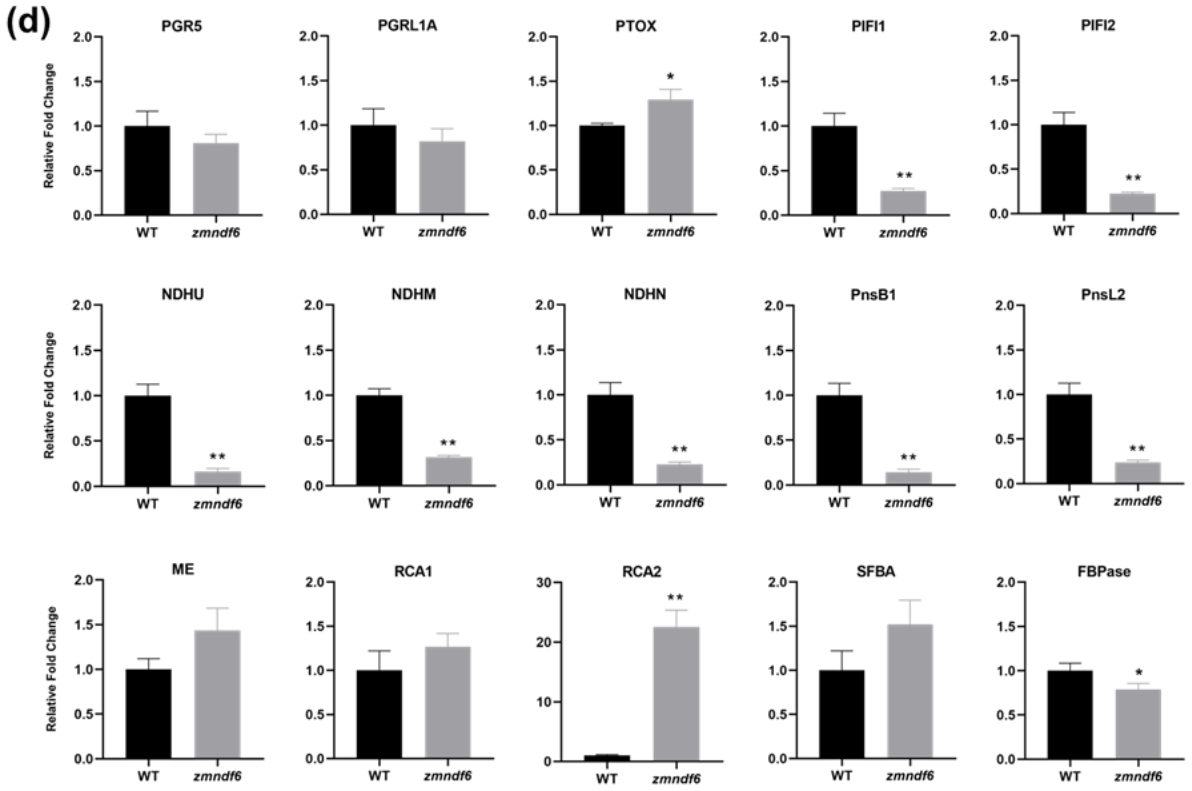

Fig. 7

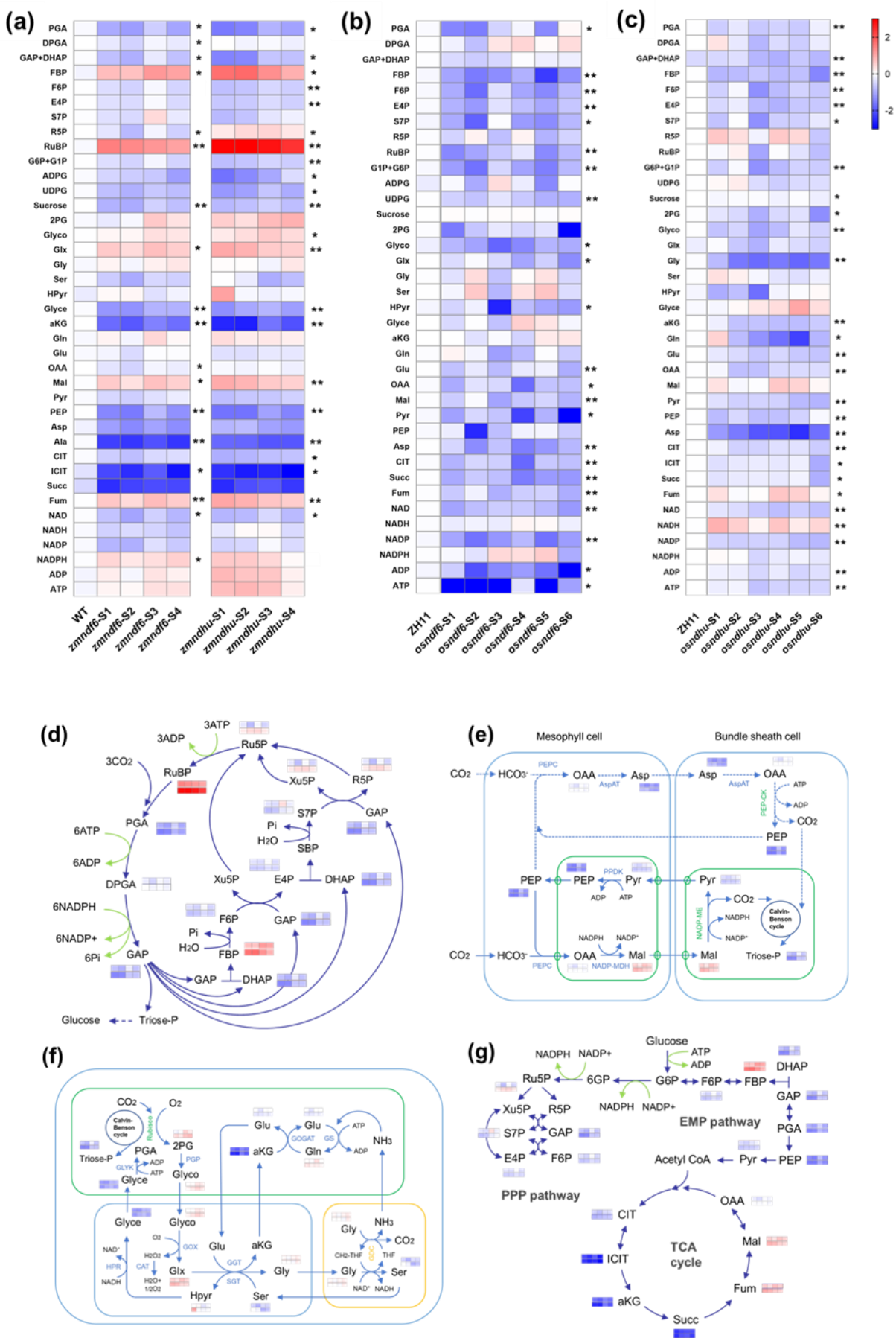

Fig. 7

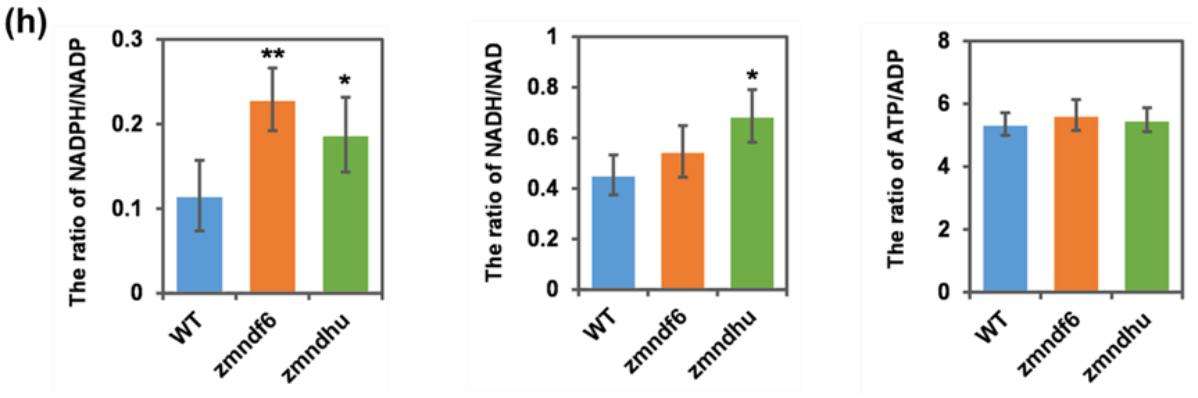

Fig. 8

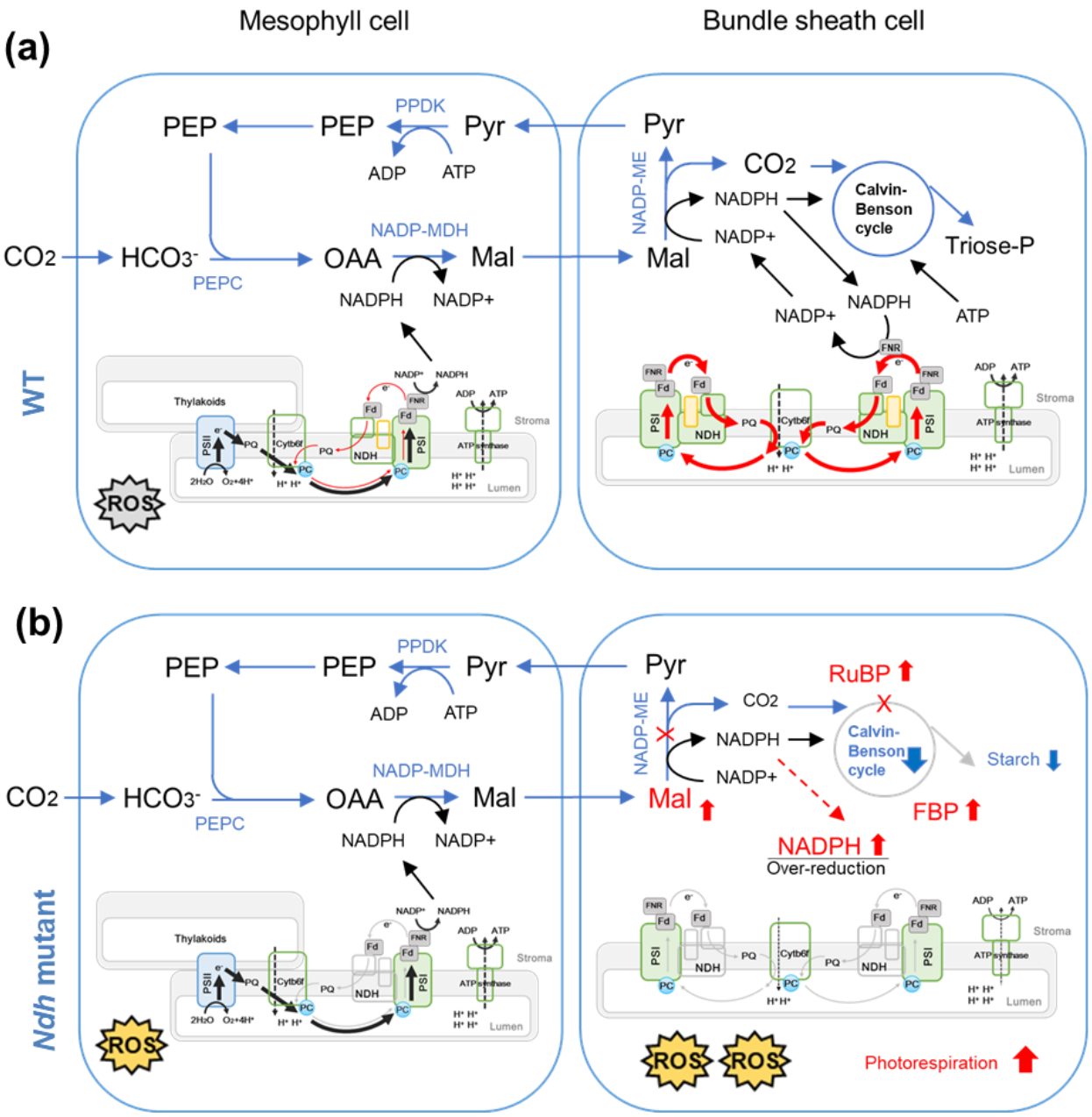

Fig. S1 Schematic model and transcript levels of NDH subunits in maize and rice

(a) Schematic model of the NDH–PSI supercomplex (Derived from Shikanai, 2015). NDF6 was renamed as PnsB4; (b) Comparison of the transcript levels of cyclic electron transport related components in maize and rice leaf gradients (Derived from Wang et al., 2014).

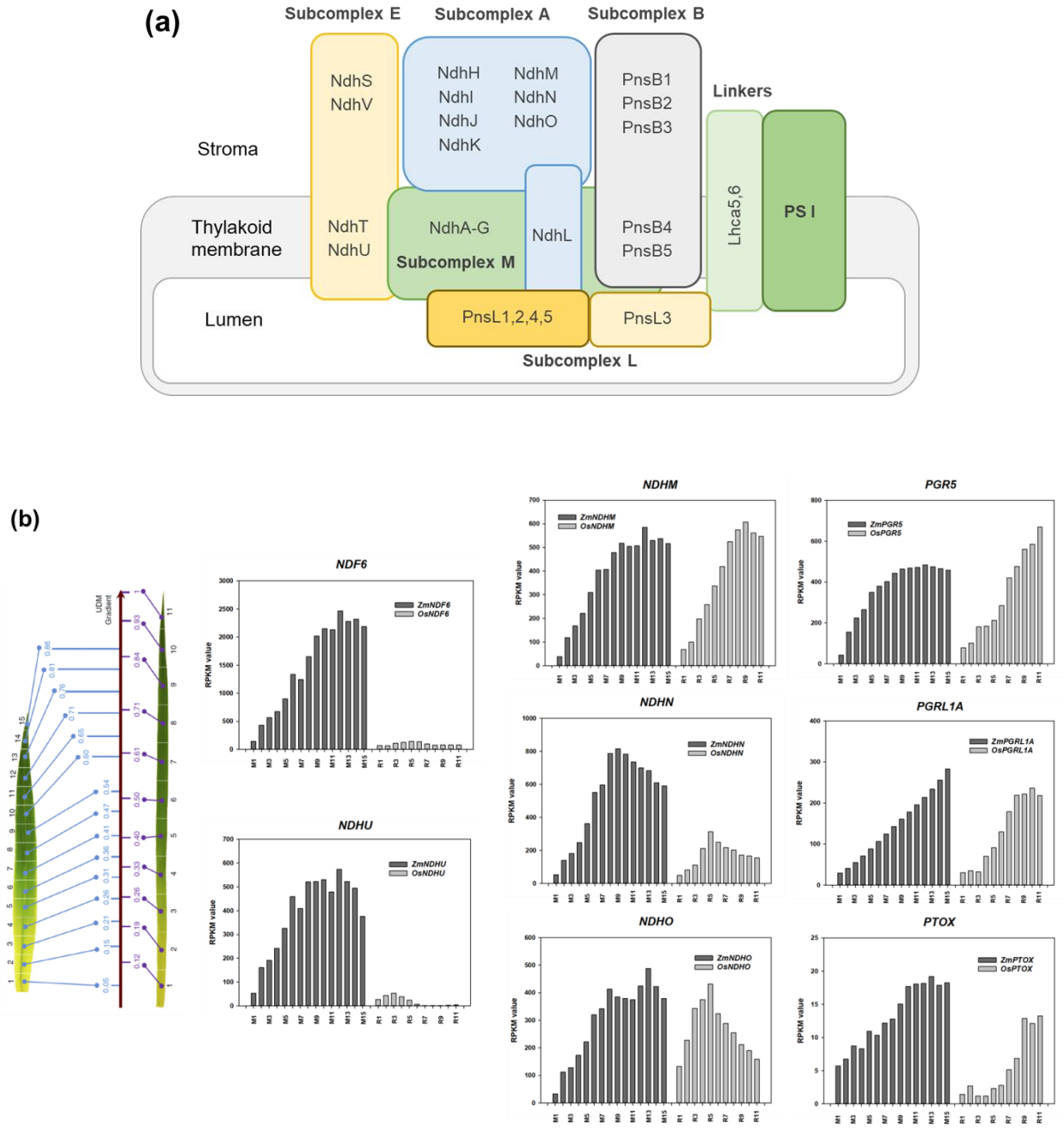

Fig. S2 Mutation of NDH genes in maize and rice with CRISPR-Cas9 technology

Schematic figures of the target sites and CRISPR-Cas9 edited sequences for (a) *ZmNDF6*, (b) *OsNDF6*, (c) *ZmNDHU*, and (d) *OsNDHU*. Nucleotides in red represent the Cas9 target site and red box indicates the difference between WT and mutants. See main text for details.

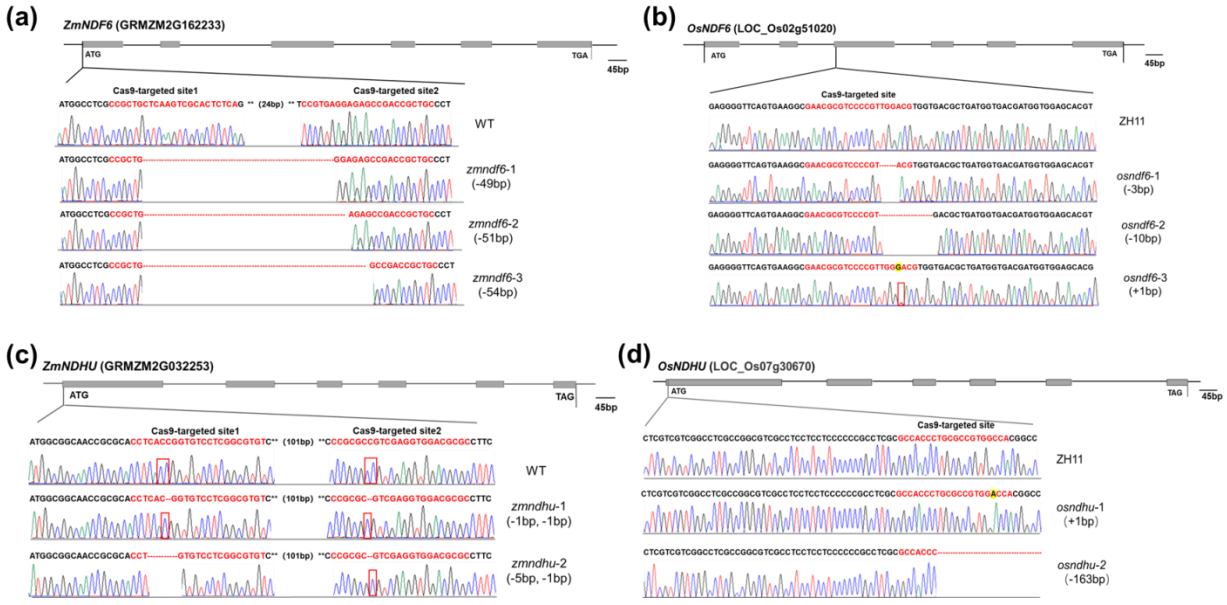

Fig. S3 The phenotypes of maize *zmndf6* and *zmndhu* mutants growing in the field greenhouse

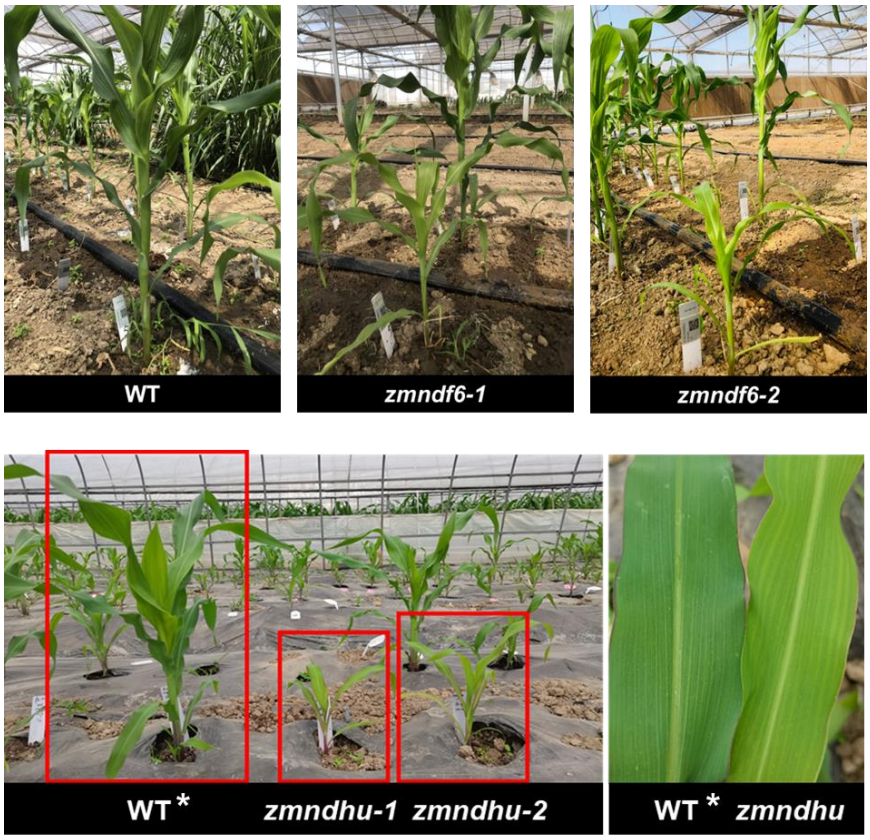

Fig. S4 Induction Kinetics and Post-illumination Increase in Chlorophyll Fluorescence in Maize Plants

The post-illumination increase of Chlorophyll fluorescence disappeared in *zmndf6* and *zmndhu* mutants, showing the inhibited activity of cyclic electron transport. The decline of Chlorophyll fluorescence under actinic light in the mutants was slower than that in the WT, indicating over-reduction of electron transport chain.

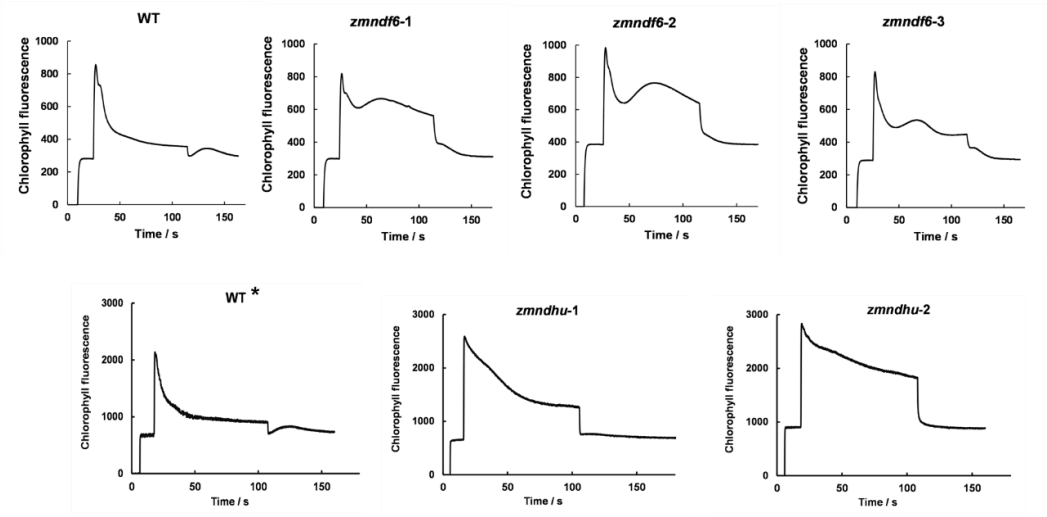

Fig. S5 Significant decrease of photosynthetic light reaction parameters in maize but not in rice *ndh* mutants

Fv/Fm (maximal PSII quantum efficiency), NPQ (non-photochemical quenching), and ETRmax (maximal electron transport rate) estimated from light response curve. Data are mean ± SE (n = 4 biological replicates). $*P < 0.05$, $**P < 0.01$ compared with WT according to Student's *t* test.

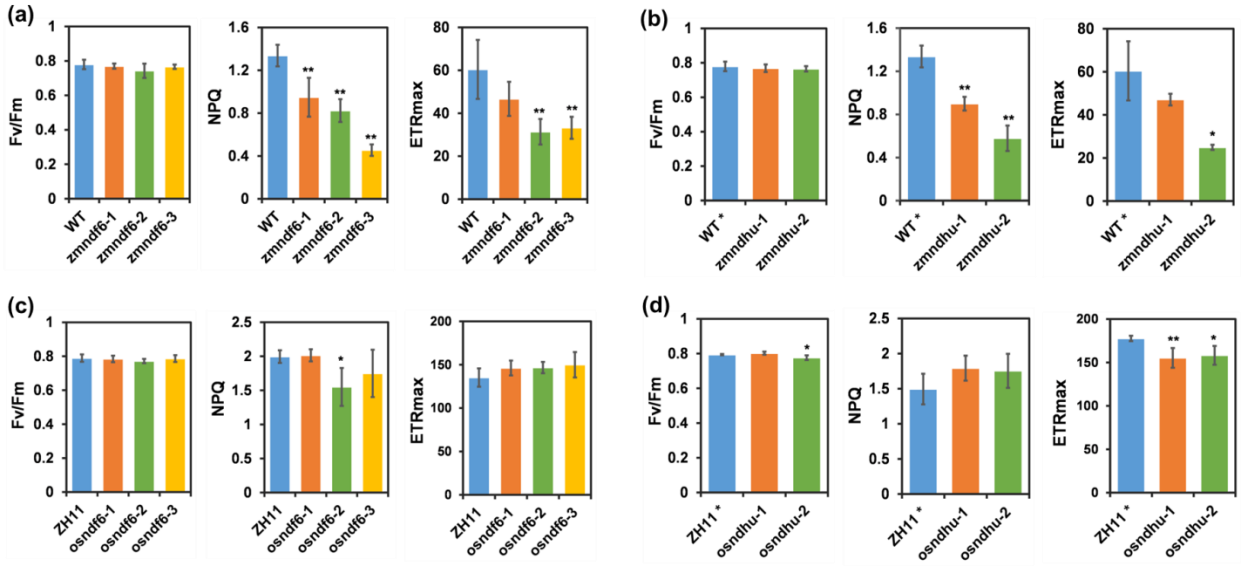

Fig. S6 Transcriptome Analysis of Maize and Rice *ndh* Mutants

(a, b) Heatmap shows differentially expressed genes related to photosynthetic linear electron transport (such as PSII, PSI, Cytb6f, ATP synthase) and cyclic electron transport in maize and rice. (c) Expression patterns of genes related to Calvin-Benson cycle, photorespiration, and C_4 pathway in maize and rice. Other pathways include starch synthesis, N-metabolism (d), transport system (e), and redox regulation (f). Heatmap data represents mean value of 3 biological replicates. *P < 0.05, **P < 0.01 compared with WT according to Student's t test.

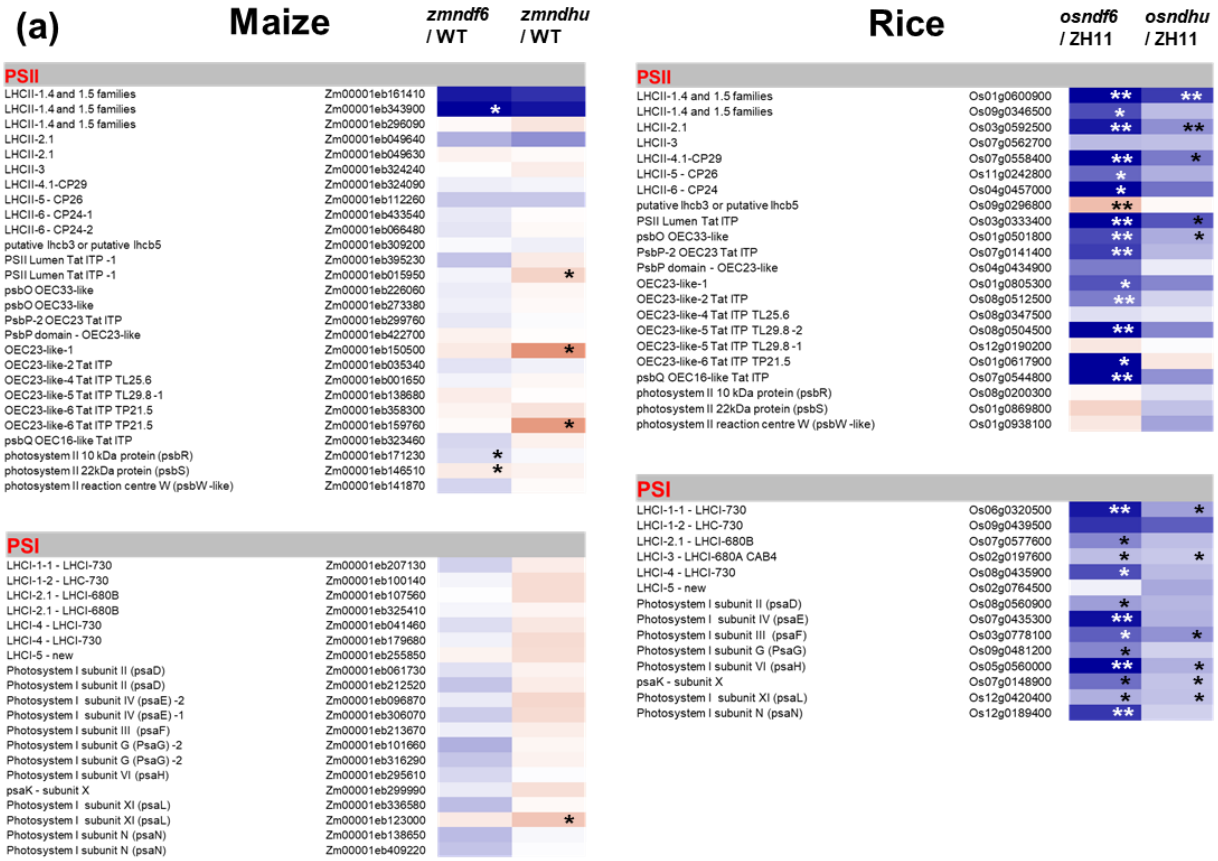

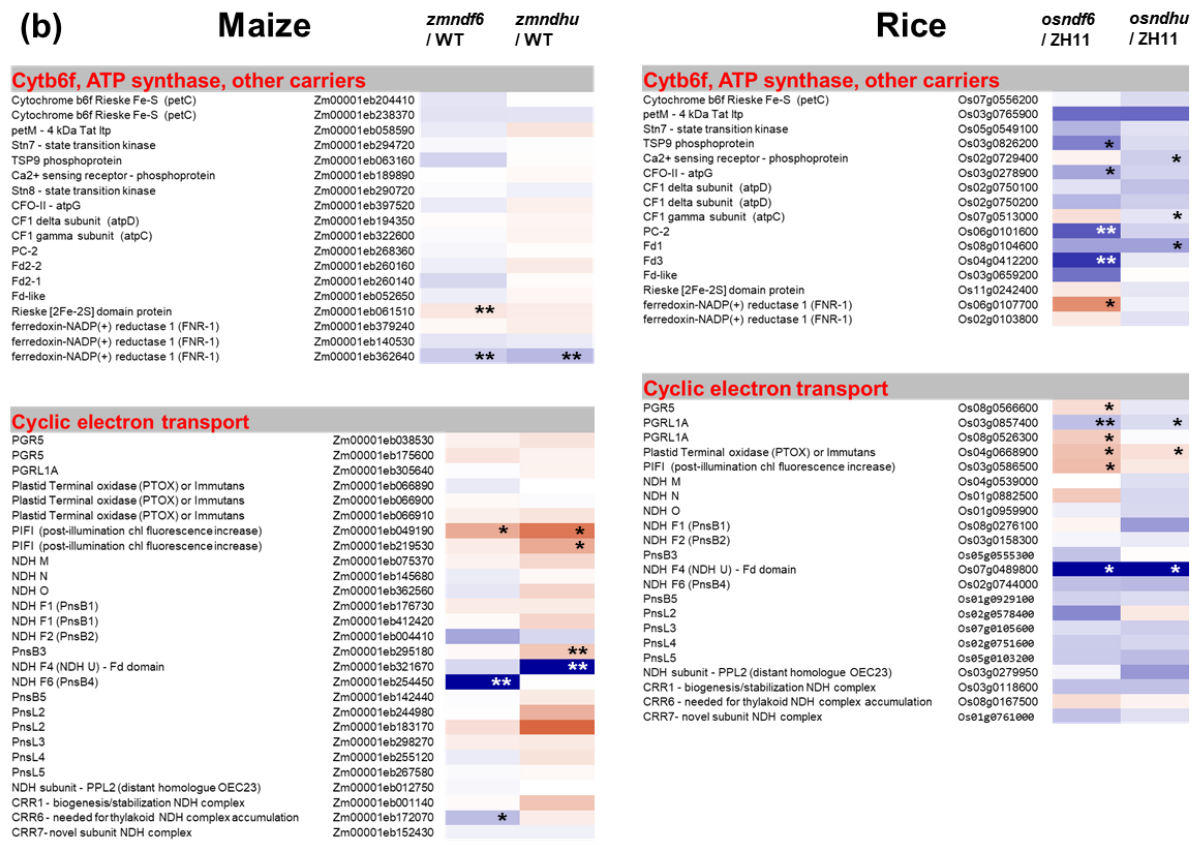

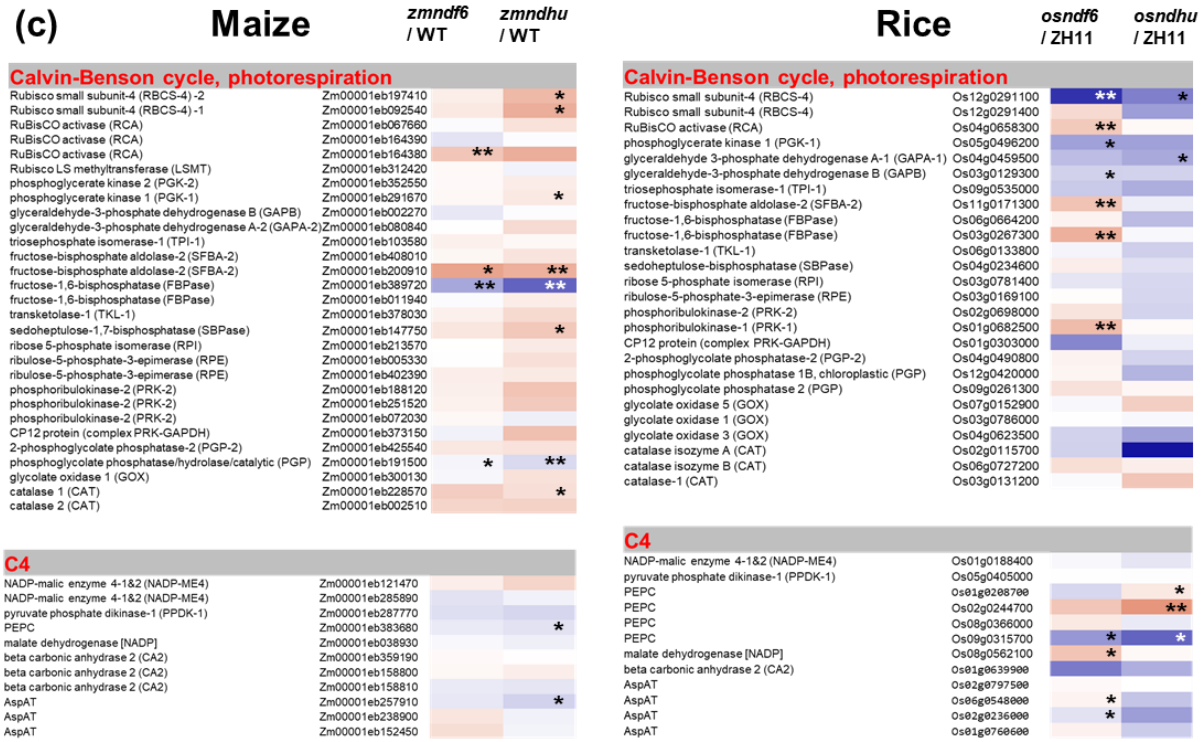

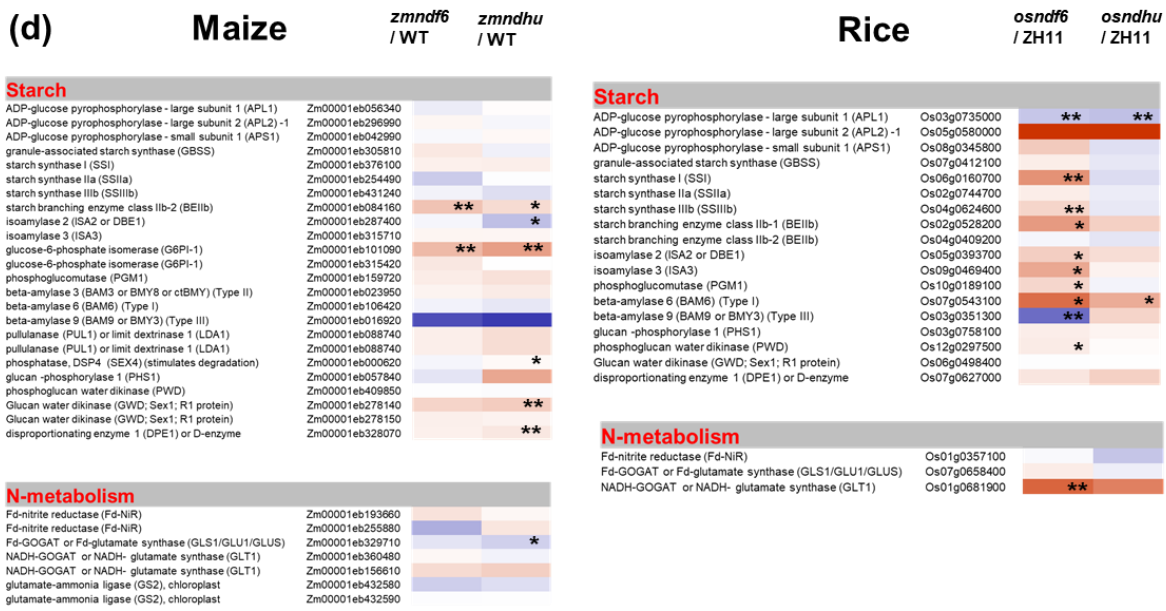

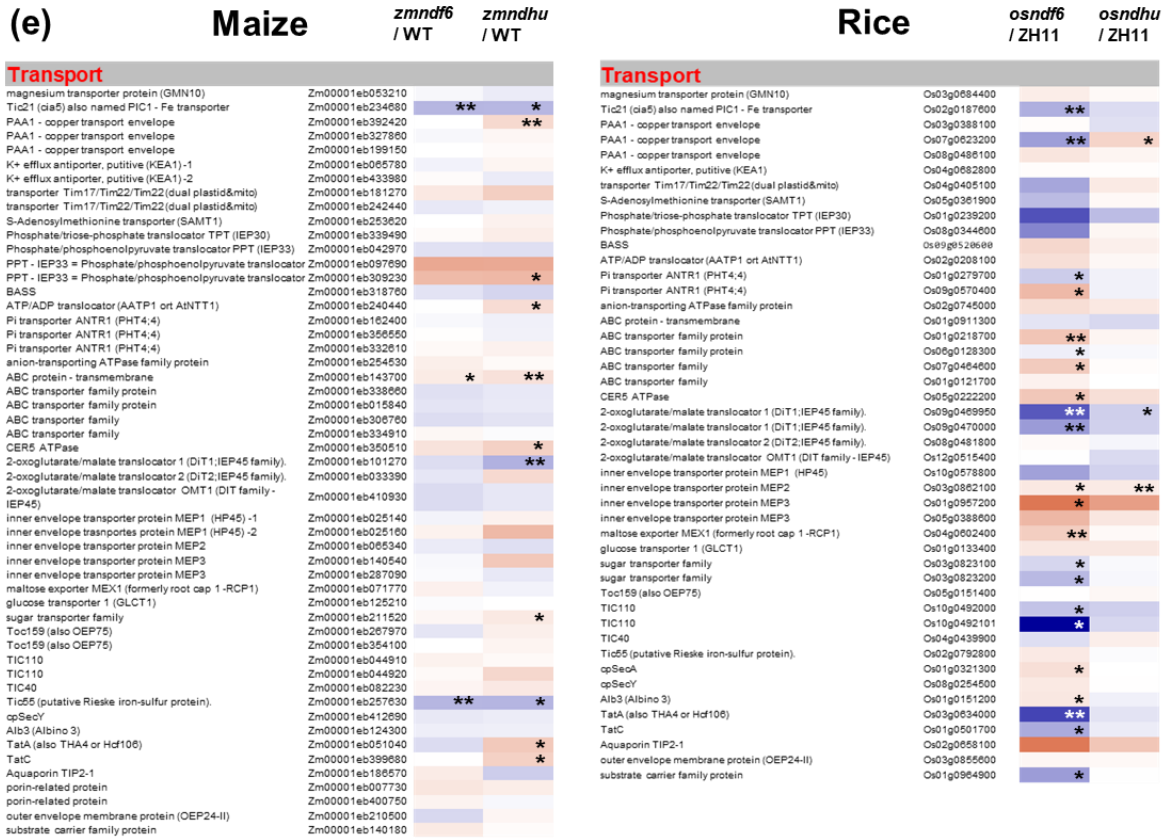

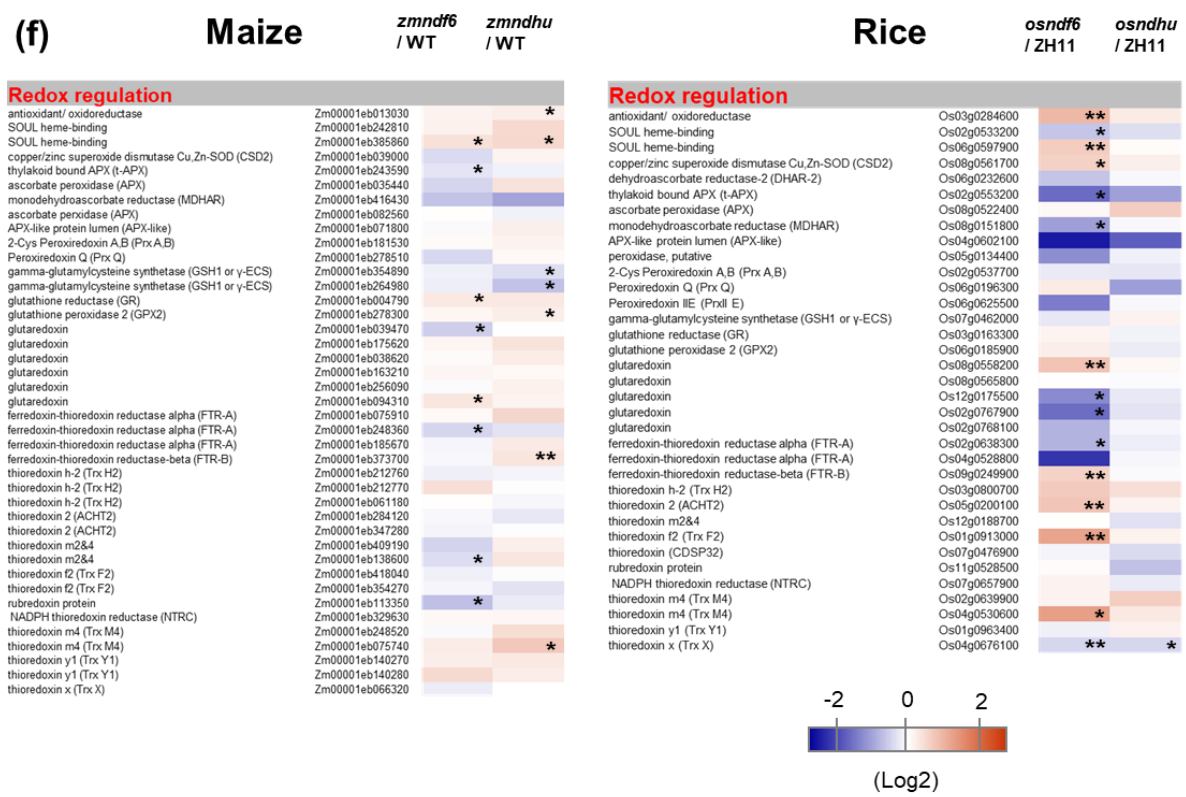

Fig. S7 Changes of BS cell protein content in maize *zmndf6* mutants

Changes of BS cell protein content related to electron transport (a), metabolism and redox (b) supplementary to Fig 6d. Comparisons were made between WT and *zmndf6* mutant according to quantitative values from BS cell proteomics. Data are mean ± SE (n = 3 biological replicates). $*P < 0.05$, $**P < 0.01$ compared with WT according to Student's t test. (c) Light microscope and immunoblot of RbcL (BS cell enriched) and PPDK (M cell enriched) to test the purity of isolated BS cell samples of WT and *zmndf6* mutant.

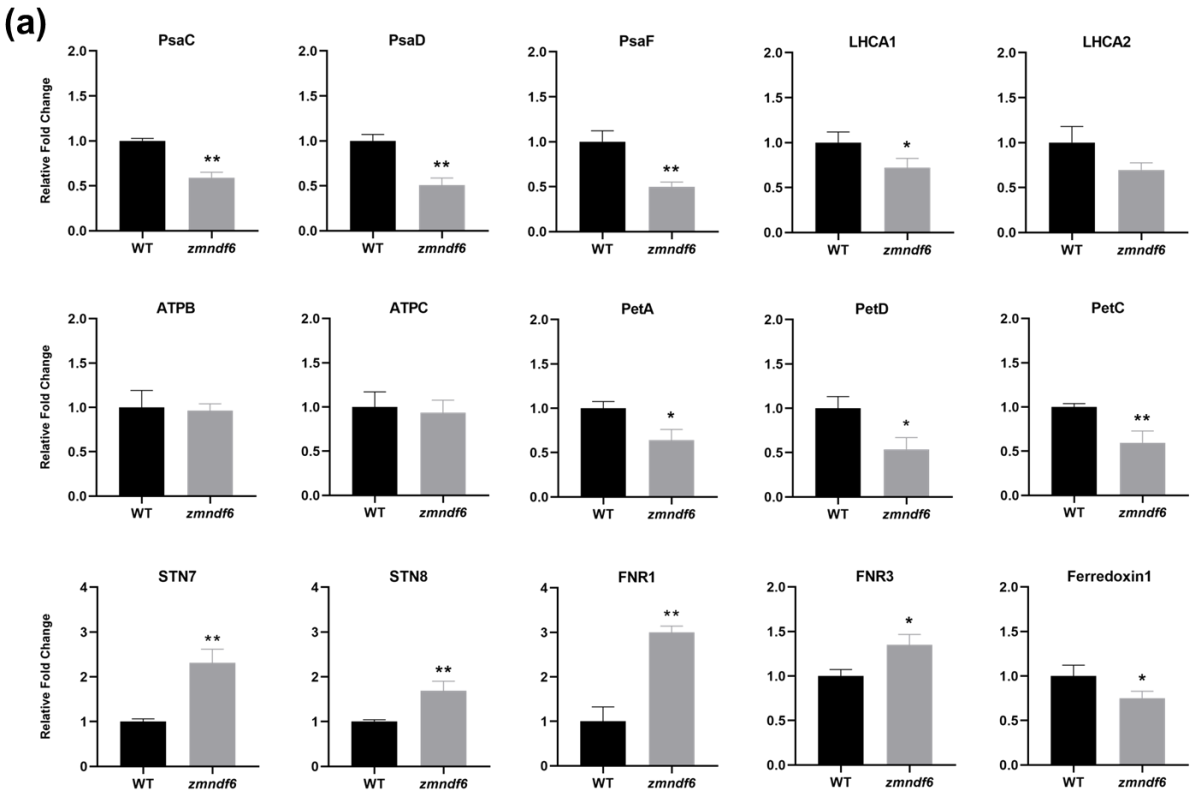

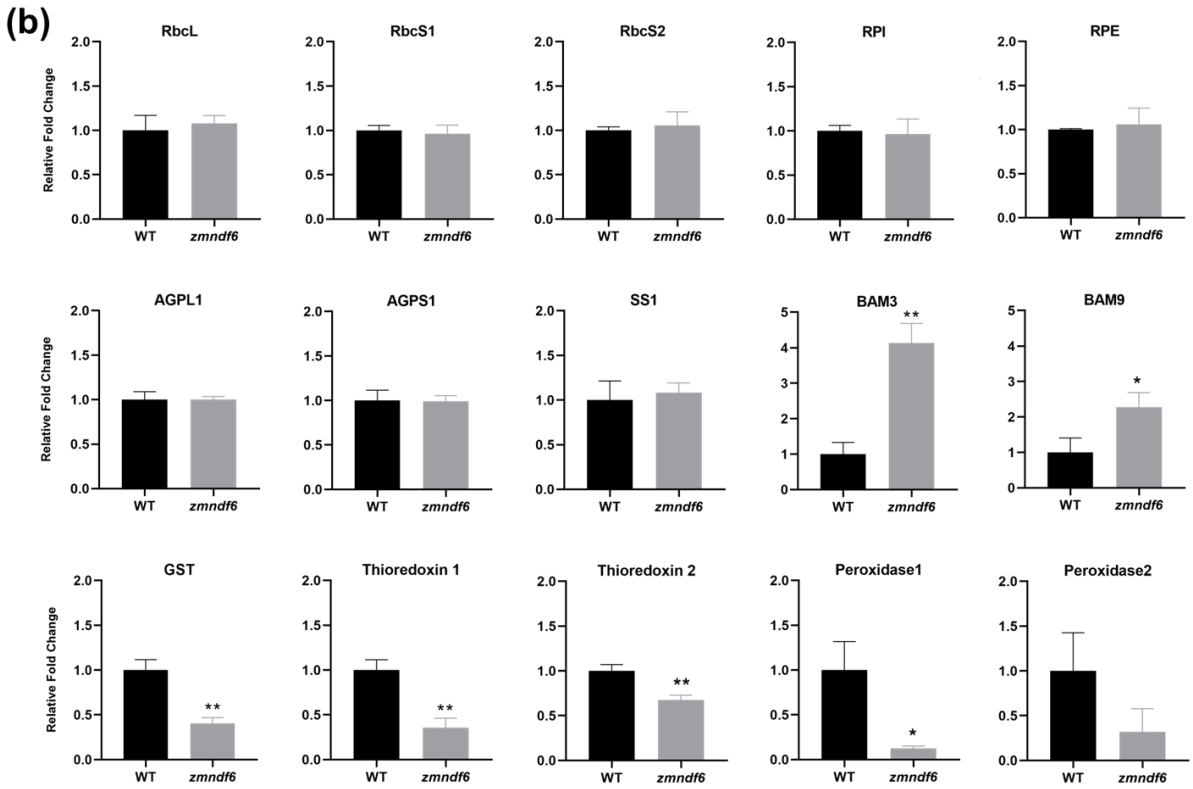

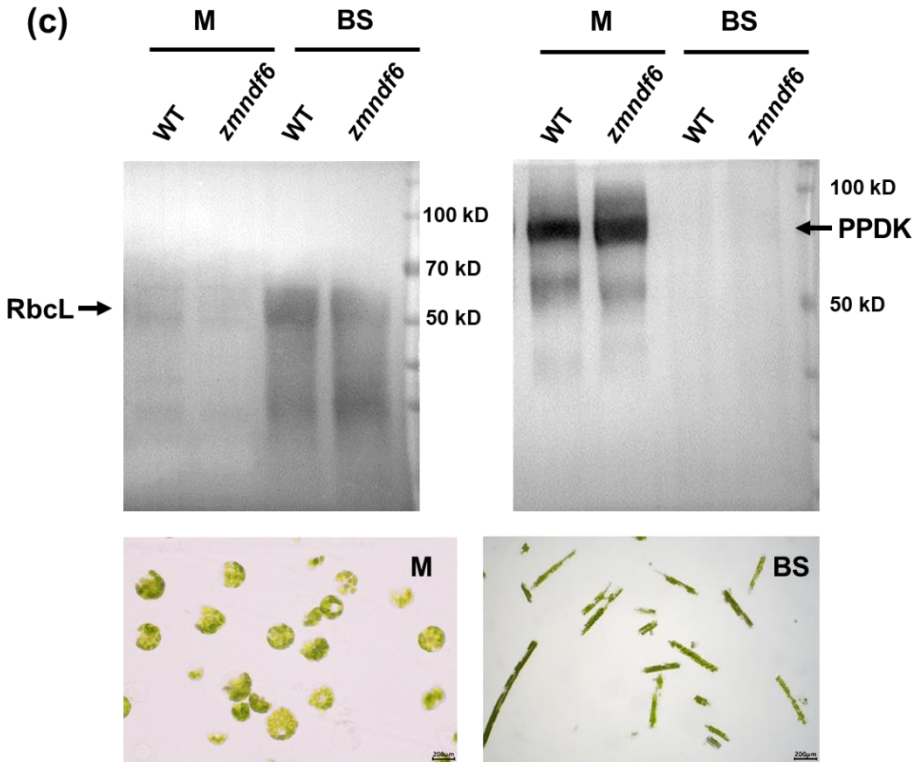

Table S1 Comparison of the BS/M ratio (mRNA or protein) of selected cyclic electron transport related components in maize

(Derived from a, Li et al., 2010; b, Majeran et al., 2008; c, Friso et al., 2010)

Name	Accession number	Bundle sheath: mesophyll ratio (mRNA)	Bundle sheath: mesophyll ratio (Protein)	
NDH subnit F6 (NDF6)	GRMZM2G162233	2.21[a]	7.58[b]	2.00[c]
NDH subnit F4 (NDHU)	GRMZM2G032253	4.26[a]	3.03[b]	2.94[c]
NDH subnit M (NDHM)	GRMZM2G109244	2.73[a]	4.23[b]	2.10[c]
NDH subnit N (NDHN)	GRMZM2G110277	3.17[a]	2.37[b]	2.13[c]
NDH subnit O (NDHO)	GRMZM2G133844	3.78[a]	2.88[b]	2.74[c]
PGR5	GRMZM2G017045	--	--	0.90[c]
PRGL1A	AC203966.5_FGP002	--		1.32[c]